

# Estimation of In Situ Stresses with Hydro-Fracturing Tests and a Statistical Method

Hikweon Lee<sup>1</sup> · See Hong Ong<sup>2</sup>

Received: 26 March 2017 / Accepted: 20 October 2017 / Published online: 28 October 2017  
© Springer-Verlag GmbH Austria 2017

**Abstract** At great depths, where borehole-based field stress measurements such as hydraulic fracturing are challenging due to difficult downhole conditions or prohibitive costs, in situ stresses can be indirectly estimated using wellbore failures such as borehole breakouts and/or drilling-induced tensile failures detected by an image log. As part of such efforts, a statistical method has been developed in which borehole breakouts detected on an image log are used for this purpose (Song et al. in Proceedings on the 7th international symposium on in situ rock stress, 2016; Song and Chang in J Geophys Res Solid Earth 122:4033–4052, 2017). The method employs a grid-searching algorithm in which the least and maximum horizontal principal stresses ( $S_h$  and  $S_H$ ) are varied, and the corresponding simulated depth-related breakout width distribution as a function of the breakout angle ( $\theta_B = 90^\circ - \text{half of breakout width}$ ) is compared to that observed along the borehole to determine a set of  $S_h$  and  $S_H$  having the lowest misfit between them. An important advantage of the method is that  $S_h$  and  $S_H$  can be estimated simultaneously in vertical wells. To validate the statistical approach, the method is applied to a vertical hole where a set of field hydraulic fracturing tests have been carried out. The stress estimations using the proposed method were found to be in good agreement with the results interpreted from the hydraulic fracturing test measurements.

**Keywords** Hydraulic fracturing · Breakout · Drilling-induced tensile fracture · In situ stress · Stress polygon

## 1 Introduction

The knowledge of in situ stresses is essential for designing underground structures for civil engineering and mining applications, developing oil and gas fields and geothermal resources, and studying faulting and earthquake mechanisms. Because stress is a tensor, not only it is characterized by its orientation and magnitude, but it is also represented by an array of components that are functions of the coordinates of a space. In situ stresses are typically represented by the three principal stresses,  $S_1$ ,  $S_2$  and  $S_3$ , which are mutually orthogonal. For practical purposes, it is often assumed that the directions of the principal stresses are approximately vertical and horizontal. Adopting this connotation, the principal stresses are represented by  $S_v$  for the vertical stress, and  $S_H$  and  $S_h$  for the maximum and minimum horizontal stresses, respectively. Throughout this manuscript, the symbol ( $S$ ) stands for total stress, while the symbol ( $\sigma$ ) stands for effective stress.

Wellbore wall rock failures such as breakouts and drilling-induced tensile fractures (DITFs), often detected in acoustic or resistivity image logs, have been successfully used as a reliable indicator for inferring in situ stress orientations (Bell and Gough 1979; Zoback et al. 1985; Haimson and Herrick 1986; Shamir and Zoback 1992; Brudy and Zoback 1999; Chang et al. 2010). The wellbore wall rock failures are schematically illustrated in Fig. 1. Borehole breakouts are diametrically opposed compressive failure zones aligned along the  $S_h$  direction in a vertical borehole drilled into an isotropic and homogeneous rock formation (Bell and Gough 1979; Zoback et al. 1985; Haimson and Herrick 1986; Chang et al.

✉ Hikweon Lee  
hklee@kigam.re.kr

<sup>1</sup> Geological Environmental Division, KIGAM,  
124 Gwahang-no, Yuseong-gu, Daejeon 305-350,  
Republic of Korea

<sup>2</sup> Baker Hughes, a GE Company, 2001 Rankin Road, Houston,  
TX 77073-5114, USA

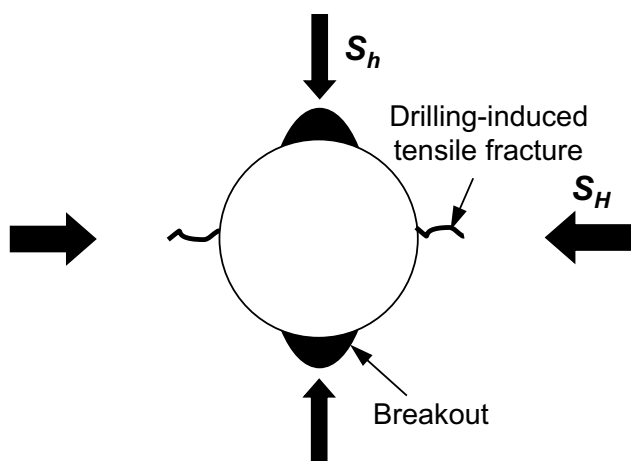


**Fig. 1** Schematic drawing of wellbore wall failures in a vertical borehole; breakouts, which are caused by shear failure, form along the direction of minimum horizontal principal stress ( $S_h$ ), and drilling-induced tensile fractures, which are caused by tensile failure, form along the direction of maximum horizontal principal stress ( $S_H$ )

2010). In contrast, excessive wellbore pressurization during drilling can induce diametrically opposed tensile fractures that form along the direction of maximum horizontal stress in a vertical borehole (Shamir and Zoback 1992; Brudy and Zoback 1999).

The estimation of overburden stress magnitude is relatively easy compared to the horizontal stresses. An overburden at a depth of interest can be estimated by integrating the density of the overlying rock formation and fluid column with depth. The minimum horizontal principal stress is most conveniently estimated by hydraulic fracturing means such as micro-fracture tests on wireline, extended leak-off tests during drilling and mini-fracture tests that precede a massive hydraulic fracturing stimulation (Haimson 1978; Baumgartner and Zoback 1989; Guo et al. 1993; Raaen et al. 2001; Raaen and Brudy 2001; Haimson and Cornet 2003). All these tests inject fluids into an isolated borehole section to induce and propagate the fractures in the surrounding rock formation. The only difference among the tests is the volume of fluid that has been injected or the size of the fracture that has been created. The pressure data recorded during the tests, particularly during the pressure falloff period, are interpreted to obtain the fracture closure pressure. The latter, being the fluid pressure recorded instantaneously when the fracture closes, is correspondingly the closest approximation of the magnitude of the minimum horizontal principal stress.

The magnitude of maximum horizontal stress ( $S_H$ ) is the most difficult to quantify because there is no direct measurement method. The commonly applied methods for constraining the magnitude of  $S_H$  include hydraulic fracture-based models and the stress polygon technique combined with wellbore failure analyses (Moos and Zoback 1990; Zoback

et al. 2003; Hickman and Zoback 2004). In the hydraulic fracturing-based method, the maximum horizontal stress is estimated from Kirsch's solution and Terzaghi's effective stress law with the assumption that the rock is perfectly impermeable (Hubbert and Willis 1957; Haimson and Fairhurst 1967; Haimson and Cornet 2003). Compared to other stress determination techniques such as overcoring, an important advantage of hydraulic fracturing is that it can be used at depths of several thousands of meters below the surface. However, its use may be limited at great depths because of either of the harsh conditions such as high temperature and pressure (Brudy et al. 1997) or cost-prohibitive operations as well as difficulties in ensuring a completely non-fluid penetrating condition.

At such great depths, the stress polygon technique combined with wellbore failure analyses may be the only viable method that can be used for constraining the maximum horizontal principal stress. The method is based on assumptions that one of the principal stresses ( $S_1$ ,  $S_2$  and  $S_3$ ) in the crust acts in the vertical direction and the others in two orthogonal horizontal directions, and the ratio of the maximum to minimum effective principal stress cannot exceed that required to cause failure (or slip) on preexisting faults that are optimally oriented in the principal stress field (Moos and Zoback 1990). If the assumptions are correct, the limiting stress ratio can be expressed by the Coulomb failure theory and assuming the cohesion of the fault planes is zero:

$$\frac{S_1 - P_p}{S_3 - P_p} = \left( \sqrt{\mu^2 + 1} + \mu \right)^2 \quad (1)$$

where  $\mu$  is the coefficient of friction of the preexisting weakness plane and  $P_p$  is the pore pressure.

The principal stresses in Eq. 1 change depending on stress regime (defined by Anderson 1951). Figure 2 illustrates the range of allowable horizontal principal stresses for the three faulting regimes using Eq. 1. The vertical line 1, which is the failure bound for the normal faulting (NF) stress environment, constrains the lowest  $S_h$  with  $S_1 = S_v$  and  $S_3 = S_h$  in Eq. 1. The inclined line 2 is the limit of the allowable stress states for the strike-slip faulting stress (SSF) field with  $S_1 = S_H$  and  $S_3 = S_h$ . The horizontal line 3 is the greatest value of  $S_H$  allowed for the reverse faulting (RF) stress environment with  $S_1 = S_H$  and  $S_3 = S_v$ . The stress states below the line of  $S_h = S_H$  are not permissible because  $S_H$  is greater than  $S_h$ . All the stress states allowed in a field are bounded within the polygon. The stress polygon becomes smaller as the pore pressure increases, while it gets larger as  $\mu$  increases.

To further constrain the possible range of horizontal principal stresses, wellbore failures (breakouts and/or DITFs) observed in the borehole are used. The line A–A' in Fig. 2 represents the stress states at which a breakout with a certain

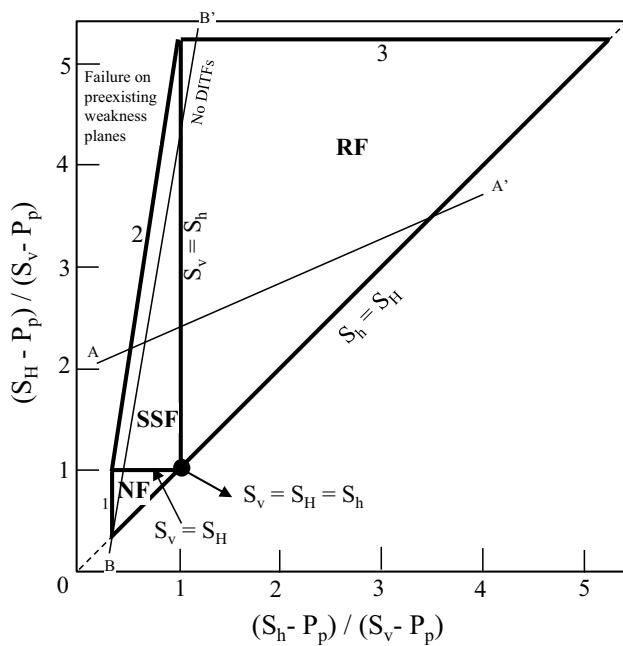


**Fig. 2** Permissible horizontal principal stresses represented by a stress polygon (thick lines). The polygon is constructed using Anderson’s faulting theory and the Coulomb failure criterion for a given coefficient of friction of a favorably oriented weakness plane, vertical stress and pore pressure. The line A–A’ represents a shear failure (i.e., breakouts) for a given breakout width and rock strength of an intact rock, and the line B–B’ represents a tensile failure (i.e., DITF) for a given tensile strength of the intact rock

width forms at the borehole wall for given rock strength parameters (uniaxial compressive strength and internal friction angle of the rock). Wider breakouts form at the stress states above the line, while narrower or no breakouts form below the line. The line B–B’ represents the stress states at which a tensile fracture is induced at the borehole wall given the tensile strength of the rock. Neglecting any thermal effects, DITFs do not form below the line but develop at the stress states above it. This method has been successfully used to characterize in situ stresses in vertical and inclined wellbores (Moos and Zoback 1990; Wiprut et al. 1997; Brudy and Zoback 1999; Hickman and Zoback 2004; Chang et al. 2010). However, using the stress polygon technique to constrain the maximum horizontal stress requires knowledge of the magnitude of minimum horizontal stress that must be determined in advance of the application.

To eliminate the need of the prior knowledge of  $S_h$  magnitude, a method that is applicable to arbitrary-oriented wellbores to constrain both horizontal principal stresses simultaneously was developed (Peska and Zoback 1995; Zoback et al. 2003; Schoenball et al. 2016). Unlike the stress polygon approach described above that uses the geometry (e.g., breakout width) of wellbore wall failures, the method uses the circumferential location of wellbore wall failures.

It is a grid-searching method that computes the difference (or misfit) of the circumferential angle between the observed and expected locations of wellbore failures for all possible stress states defined by a stress polygon and for all possible orientations of one horizontal principal stress. An advantage of this method is that it does not require information on rock strength. However, a limitation of the method is that it is only applicable to inclined boreholes because the method cannot distinguish between the different stress regimes with only the locations of wellbore wall failures.

In this paper, we first briefly describe a statistical approach originally proposed by Song et al. (2016) and Song and Chang (2017) that can be used in vertical wells to constrain the magnitude of both horizontal in situ stresses simultaneously using borehole breakout geometry. The application of this statistical method is now limited to vertical wells, so the description of this study is limited to vertical wells. We then extend the method to constrain the in situ stress magnitudes in a vertical borehole where field hydraulic fracturing tests have been conducted. By comparing the results from the statistical approach to that of field measurements, we are able to evaluate and validate the applicability and performance of the statistical methodology.

## 2 Geological Setting and Borehole (TB2) Description

The study site is located on the onshore part of the Pohang sedimentary basin, which is situated at the southeastern margin of the Korea Peninsula (Fig. 3). The sedimentary basin is a pull-apart basin formed during the back-arc opening, started during the early Miocene, of the East Sea (Chough et al. 1990; Sohn et al. 2001; Sohn and Son 2004). During the early-to-middle Miocene, the basin was extended and filled with shallow-to-deep marine deposits consisting mainly of shales and sandstones as the major lithology and conglomerates as minor. The basin-filled strata are generally dipping at less than 10° toward the East (Song et al. 2015). The basement igneous rocks and the overlaid sedimentary strata are stratigraphically separated by an unconformity.

The site has been developed at a test bed scale to study, in part, fault reactivation by CO<sub>2</sub> injection, microseismicity associated with the injection and the potential leakage risk of injected CO<sub>2</sub> along a reservoir-bounding fault. The fault, identified from a 2D seismic survey carried out at the site, has a NEE–SWW trend and dips to the NW. A vertical borehole near the fault was drilled to a depth of ~ 500 m, and a continuous whole core was extracted from the surface to the target depth. The borehole was drilled with water without any additives as a drilling fluid. After completion of the

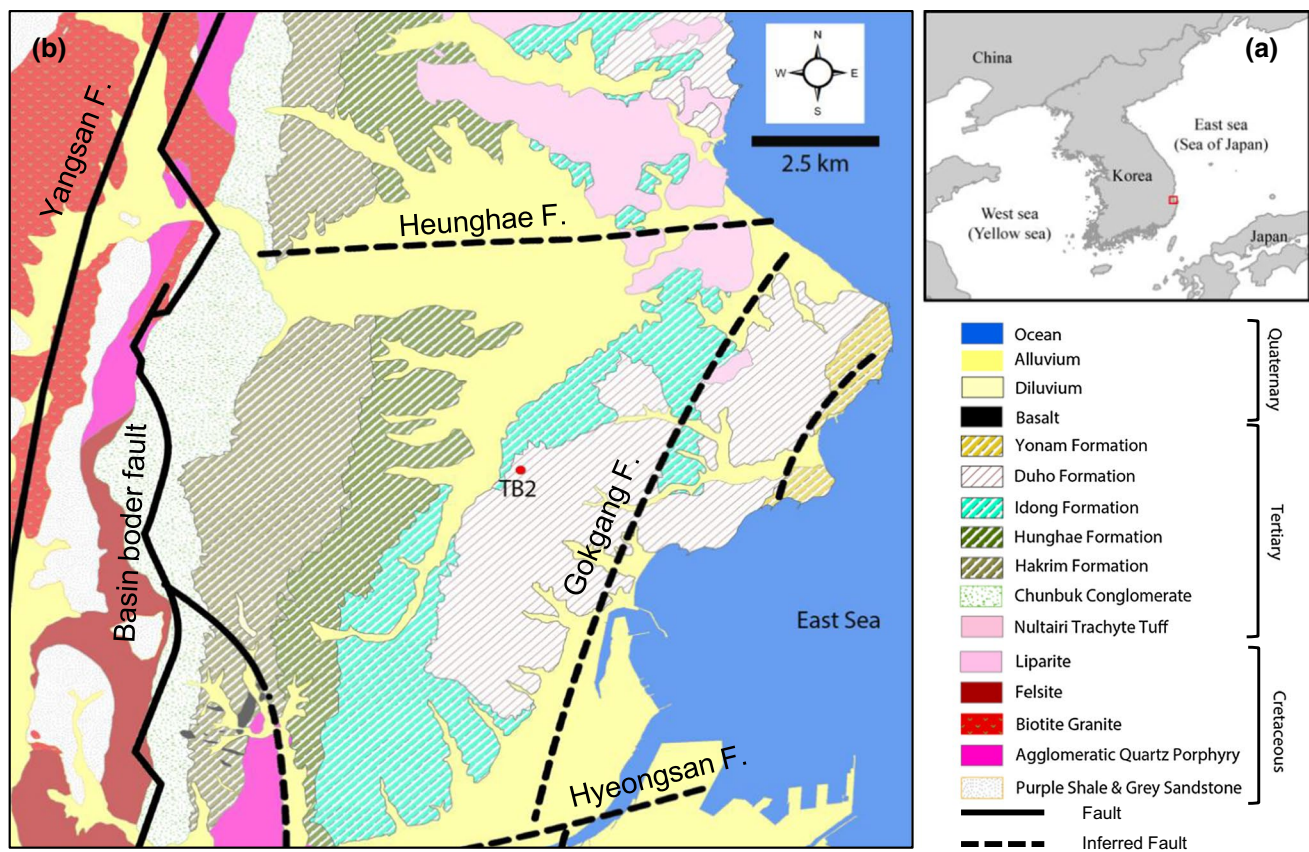


**Fig. 3** **a** Location map of the study site indicated by the red box. **b** A geological map of the surrounding area of the study borehole (TB2), showing spatial lithology distribution and major fault traces (color figure online)

drilling, a set of wireline borehole geophysical logs were run, and some of the logging data are shown in Fig. 4.

Core inspection and gamma ray log indicate that the sedimentary layers become sandier with depth (Fig. 4a). The sediments from the surface to ~ 70 m are unconsolidated, while shales are dominant from ~ 70 to ~ 300 m. Below 300 m, the lithology is predominantly sandy shales interbedded intermittently with shaly sandstone layers. Density and acoustic velocity increase with depth, but resistivity decreases with depth, suggesting that the consolidation of the sedimentary strata increases with depth (Fig. 4b–d).

### 3 In Situ Stresses Assessed by Field Measurements

#### 3.1 In Situ Stress Orientations

In most geological and geomechanical applications, the overburden stress is typically assumed to be vertical. The orientation of horizontal in situ stresses,  $S_h$  and  $S_H$ , is typically constrained in a borehole-based technique by the indicators of stress direction such as borehole breakouts and/or

drilling-induced tensile fractures (DITFs). These are rock failure features that form along the borehole due to high stresses arising from stress concentrations around the borehole as a result of replacing the rock column with a lighter drilling mud during the drilling process.

When the drilling mud weight is less than the lower limit of a safe mud weight window, a pair of diametrically opposed compressive failure zones or borehole breakouts develop. In a vertical or near-vertical wellbore, these breakouts form when the stress concentration exceeds the compressive strength of the rock align along the direction of  $S_h$  (Fig. 1).<sup>1</sup> In contrast, when the mud weight is greater than the upper limit of the mud window, a pair of diametrically opposed tensile failure or drilling-induced fractures occur along the  $S_H$  direction (Fig. 1). These stress direction indicators are typically detected by acoustic or electrical image logs run along the borehole while drilling or immediately after drilling.

<sup>1</sup> The upper limit of the mud weight window in this context is referred to as the fracture initiation pressure.

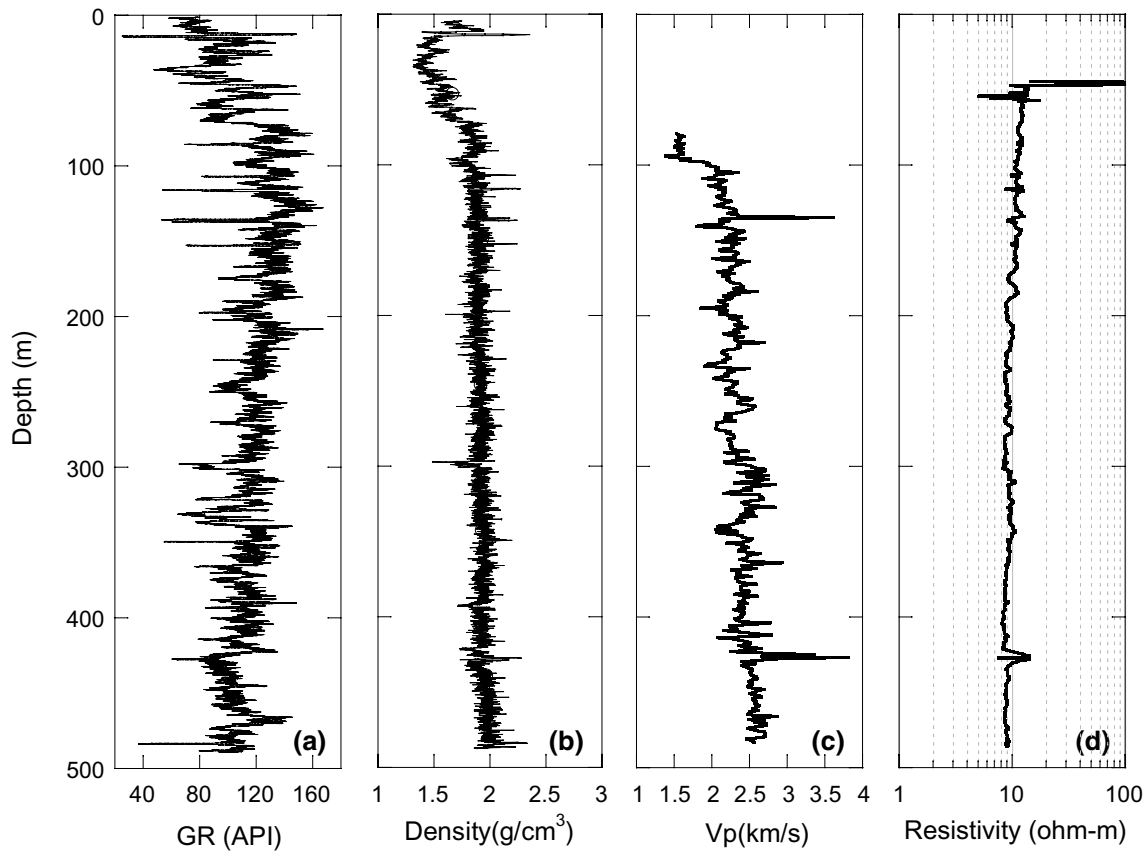


**Fig. 4** Wireline-conveyed geophysical borehole logs recorded along the study borehole (TB2). GR is the gamma ray and  $V_p$  is the P-wave velocity

As stated earlier, an acoustic borehole viewer (BHTV) was run along the study borehole immediately after the drilling (Fig. 5a). We picked the breakouts observed on the image and plotted them in Fig. 5b. These breakouts, observed from ~ 200 m to the bottom of the hole, show a consistent orientation along the borehole. By averaging the orientations of the breakouts picked, the direction of the minimum horizontal principal stress is approximately  $16.7^\circ \pm 8.8^\circ$  or  $196^\circ \pm 8.5^\circ$ . Based on this finding, we infer the direction of maximum horizontal stress to be  $\sim 107^\circ$  or  $287^\circ$ .

### 3.2 In Situ Stress Magnitudes

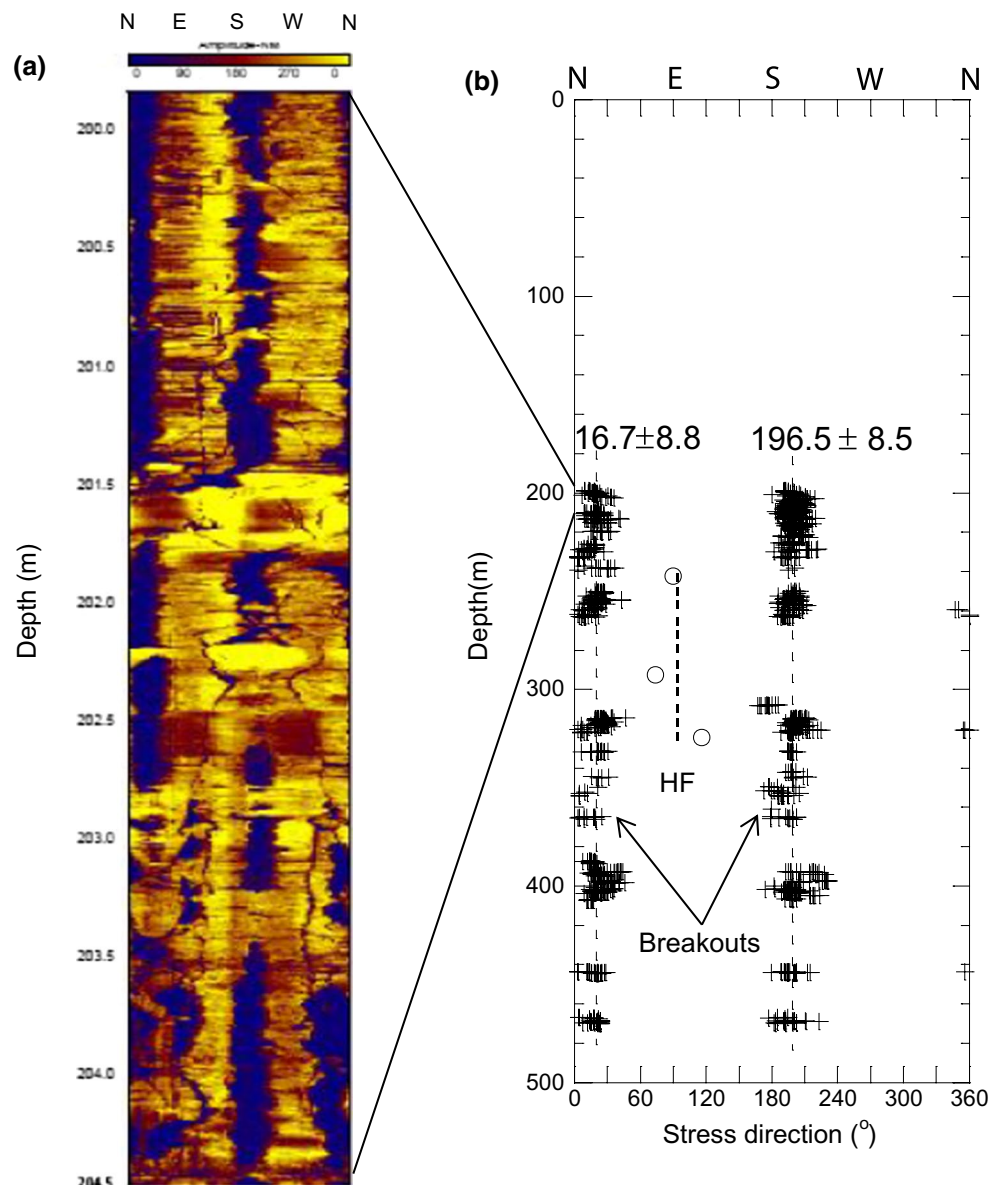
Along with the orientations of the three principal stresses, a complete characterization of the in situ stress tensor requires the determination of the stress magnitudes including pore pressure. The overburden stress is the weight of overlying rock formations and fluids acting vertically at a depth and is typically obtained by integrating the bulk density log. As shown in Fig. 4, a bulk density log is available, and cumulatively adding the weights of the overlying fluid-saturated rock formations generates a profile of vertical

stress along the study borehole. The total estimated vertical stress is shown in Fig. 6, and its gradient is approximately 17.90 MPa/km.

Pore pressure, an important component of the geomechanical model, is assumed to be hydrostatic in this study. This determination is partly based on the lack of particular overpressure signatures from the resistivity and acoustic logs (i.e., a decrease in resistivity and acoustic velocity with depth, Fig. 4), and an absence of overpressured indicators such as kicks during drilling.

To measure the magnitude of minimum horizontal principal stress ( $S_h$ ), a series of hydraulic fracturing (HF) tests were carried out at several depths along the study borehole. One advantage of the hydraulic fracturing method in measuring rock stress is that it provides a relatively reliable value of the magnitude of  $S_h$  at great depths due to a fairly large rock volume sampled. This capability makes the method ideally suited for routine measurements of the principal stress at shallow-to-deep depths. In contrast, all the other stress measurement techniques (e.g., borehole relief methods such as overcoring) are limited to depths of a few hundred meters from the surface and involve only a relatively small rock

**Fig. 5** **a** Acoustic image of the borehole recorded in a televiewer run immediately after completion of drilling. Breakouts appear as a pair of dark vertical bands that are diametrically opposed. **b** Orientations of breakouts (BOs) and hydraulic fractures (HFs) picked from the acoustic images taken along the wellbore. Breakouts are fairly consistently oriented along the borehole in the direction of  $16.7^\circ \pm 8.8^\circ$  and  $196.5^\circ \pm 8.5^\circ$ . Hydraulic fractures are formed approximately  $90^\circ$  from the breakout orientation



volume (Fairhurst 2003; Haimson and Cornet 2003; Ljunggren et al. 2003).

Prior to the tests, an acoustic borehole televiewer (BHTV) image log was run to select depth intervals of intact formations where the HF tests were then conducted. A relog of the interval was also performed to compare pre- and post-fracturing image logs and identify the induced hydro-fractures. Additionally, whole cores were thoroughly investigated to aid in the test interval selection. These pretest exercises resulted in the selection of seven depth locations (75.0, 133.0, 181.3, 242.5, 292.5, 324.5 and 368.0 m) for the in situ hydraulic fracturing tests.

Field hydraulic fracturing tests were carried out in each of the selected depth intervals, during which fluid pressure in the test interval and flow rate were monitored and recorded (Fig. 7a). Figure 7b shows hydro-fractures induced at the

selected depth of  $\sim 242$  m in the borehole. The induced HFs are subvertical, suggesting that one of the principal stresses is nearly vertical at the site. The falloff portion of pressure–time curves was analyzed to estimate the instantaneous fluid pressure in the fracture when the fracture closed ( $P_c$ ), which is equivalent to the normal compressive stress ( $S_h$ ) acting on the vertical fracture plane. In many cases, the pressure decline after pump shut-off is gradual and  $P_c$  often-times may not be distinct. Consequently, a certain amount of interpretation is involved in analyzing the pressure decline curves to identify the closure pressure. Several graphical interpretation methods have been proposed and used to estimate  $P_c$  from the pressure–time curves (Gronseth and Kry 1983; Enever and Chopra 1986; Doe et al. 1983; Zoback and Haimson 1982). Although considered to be subjective, the graphical interpretation techniques provide a reasonable

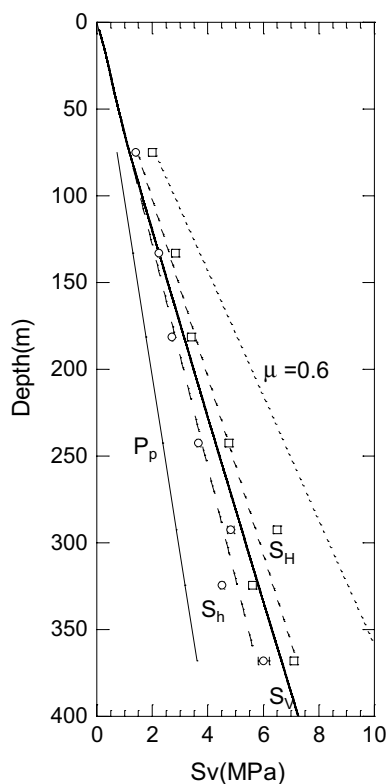


**Fig. 6** A profile of in situ stresses ( $S_v$  = vertical stress,  $S_H$  = maximum horizontal stress,  $S_h$  = least horizontal stress and  $P_p$  = pore pressure) as a function of depth along the study borehole.  $\mu$  is the friction coefficient of faults

approximation of  $P_c$  in many cases, albeit uncertainties remain in the interpretation of the pressure data. In an effort to reduce subjectivity in the determination of  $P_c$ , Lee and Haimson (1989) suggested a statistical approach.

In this study, we employed the bilinear pressure decay method (Fig. 8a) proposed by Lee and Haimson (1989) to determine  $P_c$  from the pressure decline records. The closure pressures estimated using the method are plotted against pressurization cycles as shown in Fig. 8b. Except at two depth intervals (181 and 242 m), closure pressures in general gradually decreased and then stabilized with the number of pressurization cycles. The same phenomenon of closure pressures decrease with sequential cycles had also been observed in other works (Gronseth and Kry 1983; Baumgartner and Zoback 1989; Lee 1991; Chang et al. 2013). This phenomenon can be attributed to several reasons. A main reason among them is that the fractures induced in the first cycle did not extend far beyond the stress concentration zone around the borehole (Fig. 9). With repeating pressurization cycles, the fractures continued to propagate further into the rock formation and eventually extended far enough from the borehole to fully sense the in situ least principal stress acting normal to the fracture planes (Fig. 9, Gronseth and

Kry 1983). Another plausible reason is that as the fracture extended, its normal stiffness was reduced (Baumgartner and Zoback 1989) and a lower fluid pressure was required to keep the fracture open.

To arrive at the best estimation of the least horizontal principal stress from the closure pressures estimated at the different pressurization cycles, Gronseth and Kry (1983) took the minimum value of the closure pressures. On the other hand, Baumgartner and Zoback (1989), Lee (1991) and Chang et al. (2013) averaged the closure pressures from the multiple pressurization cycles and used the average value as the best estimation of the  $S_h$ . In this study, the estimated closure pressures remained relatively constant throughout the pressurization cycles (Fig. 8b). This indicates that the fractures induced in the first cycle have extended beyond the stress concentration region around the borehole. With this in mind, we took the averaged value of the closure pressures from multiple cycles as  $S_h$ . The profile of the least horizontal principal stress determined in this way is shown in Fig. 6. The average total  $S_h$  gradient and the ratio of  $S_h$  to  $S_v$  are approximately 15.67 MPa/km and 0.875, respectively.

The magnitude of maximum horizontal stress ( $S_H$ ) is the most difficult to quantify because there is no direct measurement method. To the author’s knowledge, there are two conventional HF criteria to establish equations between the breakdown pressure ( $P_b$ ) and in situ horizontal stresses. One (H–W criterion, Eq. 2) is based on elastic theory for impermeable rock formations (Hubbert and Willis 1957). The estimation of  $S_H$  magnitude in a perfectly impermeable elastic formation is typically made using the well-known Kirsch’s solution applied to a vertical borehole. Hubbert and Willis (1957) proposed using the fracture initiation equation (Eq. 2), which is based on Kirsch’s solution and Terzaghi’s effective stress law:

$$S_H = 3S_h - P_b - P_p + T \tag{2}$$

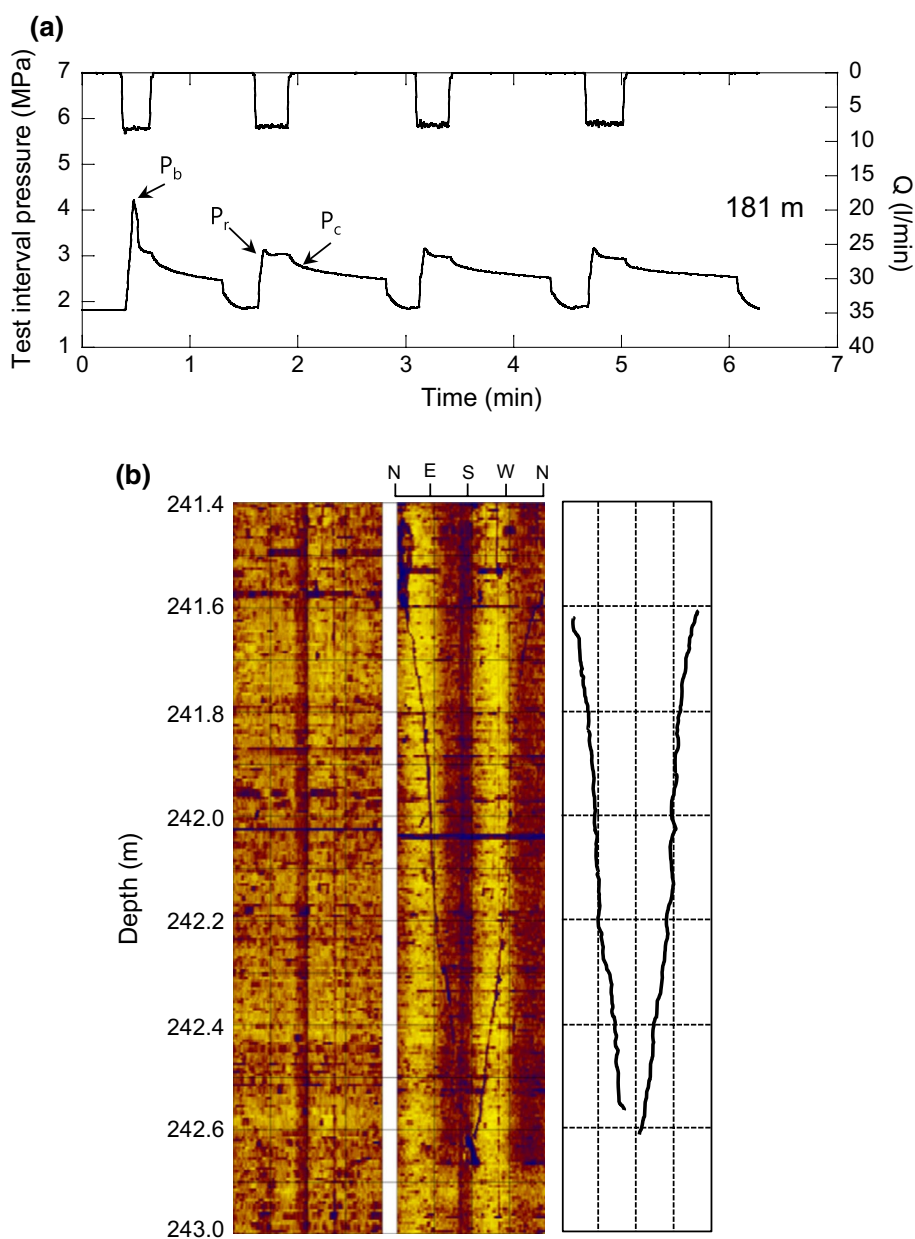
where  $P_b$  is the fracture initiation pressure and  $T$  is the tensile strength of the rock. The other (H–F criterion, Eq. 3) is based on poroelastic theory for permeable formations (Haimson and Fairhurst 1967). The poroelastic stress induced by fluid flow into surrounding rocks is considered in the H–F criterion:

$$P_b - P_p = \frac{T + 3S_h - S_H - 2P_p}{2 - 2[\alpha(1 - 2\nu)/2(1 - \nu)]} \tag{3}$$

where  $\alpha$  is the Biot’s coefficient and  $\nu$  is the Poisson’s ratio.

The estimation of total  $S_H$  using Eqs. 2 and 3 requires that the closure pressure ( $P_c = S_h$ ), the fracture initiation pressure, and the tensile strength and other properties of the rock are known a priori. The fracture initiation pressure is relatively easy to determine from the first pressurization cycle. However, the tensile strength of rock, measured by conducting either hollow cylinder tests, direct tension

**Fig. 7** **a** Pressure versus time and flow rate versus time plots recorded during the hydraulic fracturing tests at 181 m depth.  $P_b$  is the breakdown pressure,  $P_r$  is the reopening pressure, and  $P_c$  is the closure pressure. **b** Images of an acoustic borehole televiewer taken before (left) and after (middle) the field hydraulic fracturing tests, and the trace of the induced fractures (right)



tests or Brazilian tests when cores are available, is known to be loading (or pressurization) rate- and hole size-dependent (Haimson and Zhao 1991; Schmitt and Zoback 1992; Yamashita et al. 2010; Chang et al. 2013; Jensen 2016).

Due to the uncertainty associated with pressure rate and borehole size dependency in the determination of the tensile strength of rock, it is sometimes preferable to use the fracture reopening pressure for the stress computations. Bredehoeft et al. (1976) proposed using the fracture reopening pressure equation (Eq. 4) to estimate  $S_H$ :

$$S_H = 3S_h - P_r - P_p \quad (4)$$

where  $P_r$  is the reopening pressure. We employed the equation proposed by Bredehoeft et al. (1976) (Eq. 4) to estimate

the total maximum horizontal principal stress. From Eq. 4, the key pressure parameters required are the closure and fracture reopening pressures. The latter was determined from the second or third pressurization cycle by plotting pressure versus cumulative injected volume and using the graphical technique as shown in Fig. 8c. The estimated total  $S_H$  magnitudes at all the test stations are plotted as a function of depth as shown in Fig. 6. The average total  $S_H$  gradient and the ratio of  $S_H$  to  $S_v$  are 19.74 MPa/km and approximately 1.10, respectively. The relative magnitude of the three principal stresses determined indicates that the stress regime at the study site is of strike-slip faulting ( $S_H > S_v > S_h$ ).



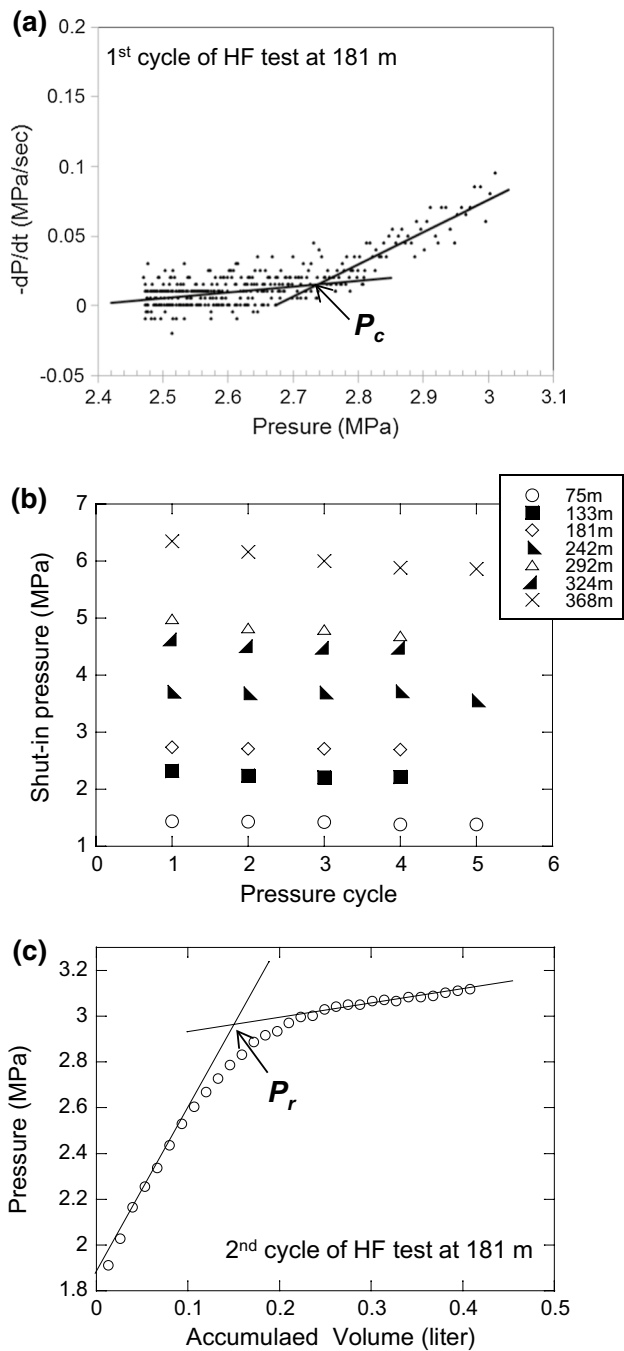


**Fig. 8** a Instantaneous closure pressure ( $P_c$ ) determined using the bilinear pressure decay rate method ( $-dP/dt$  vs.  $P$ ) proposed by Lee and Haimson (1989). b Variations of closure pressure with pressurization cycles. c Reopening pressure ( $P_r$ ) determined by means of pressure vs. cumulative injected water volume

## 4 In Situ Stress Characterization by Stochastic Analysis

### 4.1 Methodology

Wellbore wall rock failures such as breakouts and DITFs have been used to indirectly constrain the magnitudes of both horizontal principal stresses ( $S_h$  and  $S_H$ ) in vertical and inclined boreholes (Moos and Zoback 1990; Peska and Zoback 1995; Wiprut et al. 1997; Zoback et al. 2003). One of the approaches uses the stress polygon combined with wellbore failure features (Moos and Zoback 1990; Zoback et al. 2003). In this technique, a stress polygon, constructed using Anderson’s faulting classifications and Coulomb’s failure criterion ( $\tau = \mu\sigma_n$ , cohesion is assumed to be zero) for given a coefficient of friction of the pre-existing planes of weakness ( $\mu$ ), overburden stress and pore pressure, represents a range of possible in situ stress states at great depths. The coefficient of friction of preexisting weakness plane ranges from 0.6 to 0.85 (Byerlee 1978). The stress polygons as shown in Fig. 10a and b are built with a friction coefficient ( $\mu$ ) of 0.6, an overburden stress ( $S_v$ ) of 35.7 MPa and a pore pressure ( $P_p$ ) of 20.7 MPa. Depending on the in situ stress regime in the field, Fig. 10a and b indicates that the possible range of in situ stresses ( $S_h$  and  $S_H$ ) is limited by the stress polygon for this vertical well. In other words, a state of stress outside the polygon is not feasible because faulting will occur prior to reaching the stress level, and the release of the accumulated energy will return the state of stress to within the polygon.

By combining observations of wellbore failures and rock strength data with their uncertainties, the horizontal principal stresses can be further constrained. The shear wellbore failure analysis is carried out with the Coulomb failure criterion or others. Here we employ the Coulomb criterion. For example, if only borehole breakouts are observed in a vertical borehole drilled in an area of a strike-slip faulting stress regime, the possible magnitudes of horizontal principal stresses are limited within the zone indicated by the hatched polygon ABCD in Fig. 10a. (The dashed and solid lines in Fig. 10a are constructed with a breakout width,  $\theta_b = 50^\circ$ , a wellbore pressure,  $P_m = 24.8$  MPa, unconfined compressive strength of the rock,  $C_0 = 17.7\text{--}23.7$  MPa, and internal friction angle of the intact rock,  $\phi = 25^\circ$ .) Increasing the wellbore pressure ( $P_m$ ) from 24.8 to 29.0 MPa while keeping the other parameters unchanged results in the shift of the failure lines (see the dashed and solid lines located above the previous lines, Fig. 10a). The shifted lines have the same slope, but the region of possible stress states (the dotted polygon EFGH) is narrower than the previous one. This is because increasing the wellbore pressure causes an increase in the effective radial stress,  $\sigma_{rr} = \Delta P (= P_m$

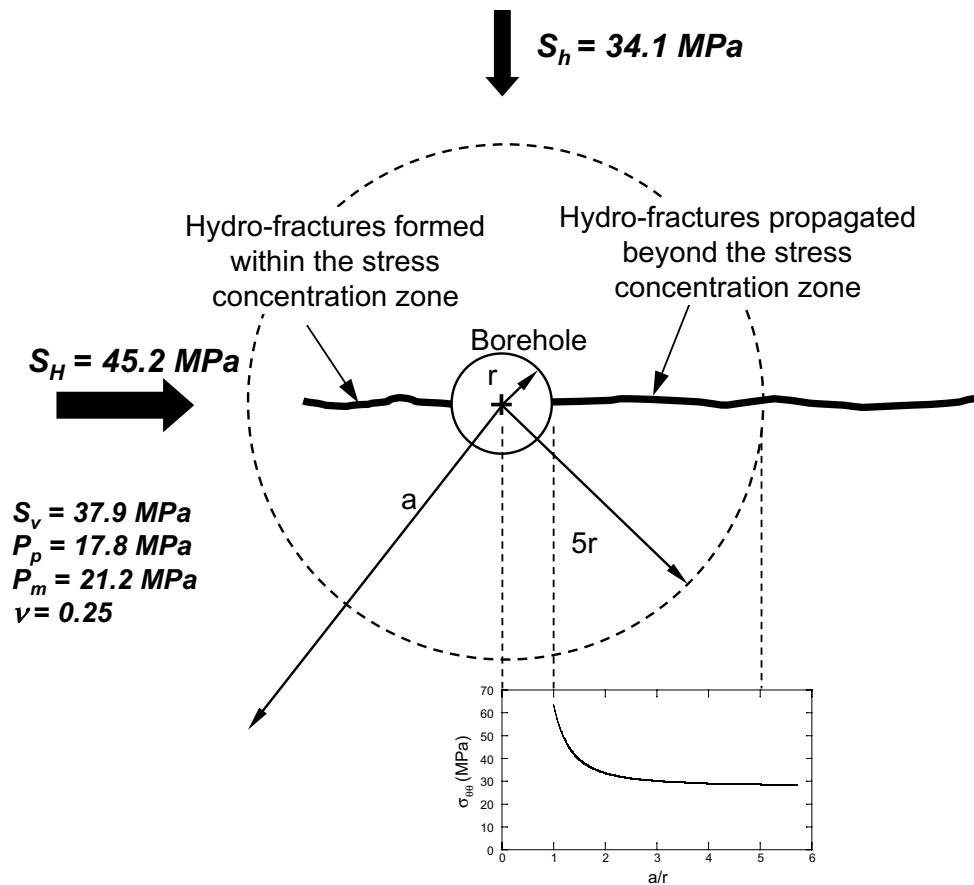


**Fig. 9** Effective tangential stress ( $\sigma_{\theta\theta}$ ) distribution along the  $S_H$  direction in a vertical borehole. The stress disturbance induced by drilling a vertical hole diminishes with radial distance and disappears approx-

imately 5 radii away from the borehole or when  $a/r = 5$ . The induced HF's need to be propagated further beyond the stress concentration zone to sense the far-field minimum horizontal principal stress ( $S_h$ )

–  $P_p$ ), and hence the rock strength as well as a reduction in the effective tangential stress, all of which contribute to limiting the formation of breakouts. Thus, for breakouts with the same width ( $\theta_b = 50^\circ$ ) to be developed, the horizontal stress anisotropy must be increased.

If only drilling-induced tensile fractures are observed at the same depth in the borehole, the horizontal principal stresses are confined within the hatched polygon A'B'C'D' in Fig. 10b. (The dashed and solid lines in Fig. 10b are constructed with a wellbore pressure,  $P_m = 24.8$  MPa, and the tensile strength of the rock is assumed to range from 0 to 10 MPa.) The tensile failure analysis is carried out with Eq. 2. Again, increasing the wellbore pressure from 24.8 to 29.0 MPa shifts the two failure lines downward but with their slopes maintained. As in the case of breakouts, the region of possible stress states (the dotted polygon E'F'G'H') becomes narrower, indicating that the increase in effective radial stress by increasing the wellbore pressure reduces the effective tangential stress. This reduction in tangential stress translates into a lower horizontal stress anisotropy which is required to cause DITFs at the borehole wall.

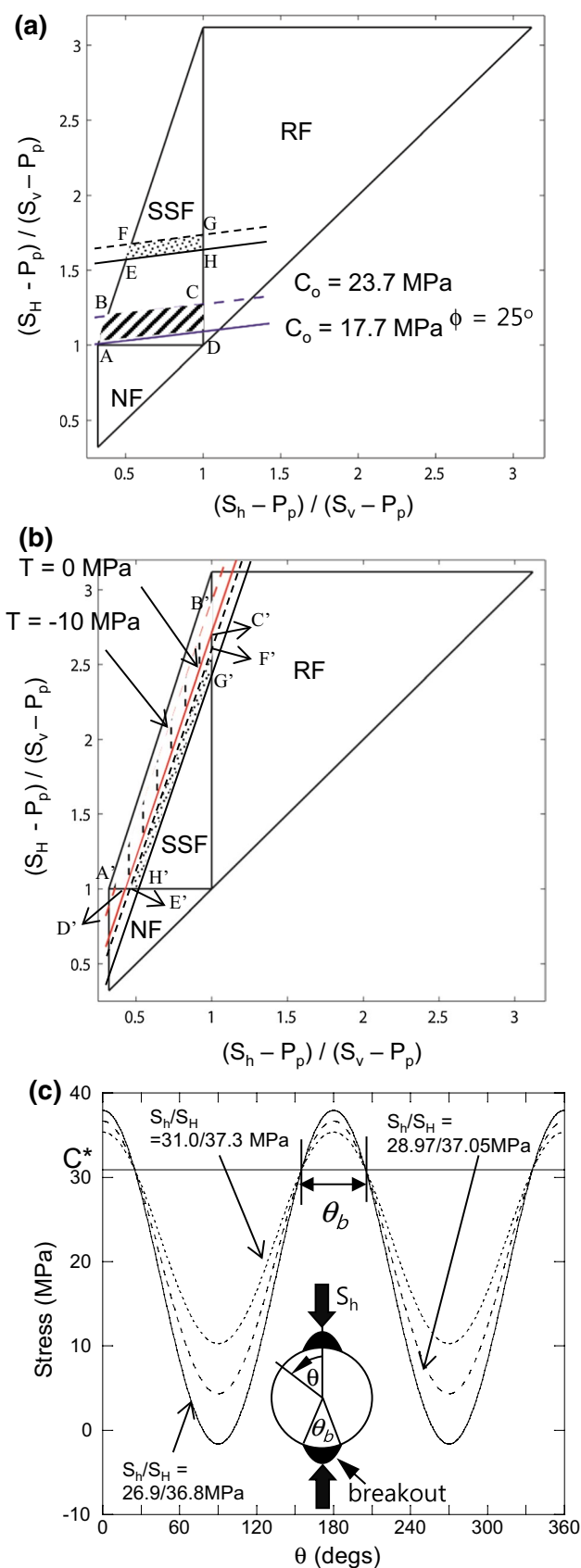
In both cases (Fig. 10a, b), knowledge of the magnitude of the least horizontal stress ( $S_h$ ) in advance from field measurements such as extended leak-off tests (XLOT) and/or wireline-conveyed micro-fracture tests would significantly reduce the possible range of the maximum horizontal stress state. Conversely, if the magnitude of the minimum horizontal stress is not known a priori, the wide range of possible stress values, as shown in Fig. 10a, b, would make constraining the stress magnitudes difficult in the vertical wellbore. This is illustrated in Fig. 10c. It shows the variation of tangential stress ( $\sigma_{\theta\theta}$ ) as a function of the circumferential angle ( $\theta$  measured from  $S_h$ ) around the borehole.  $C^* [= C_0 + \sigma_3 \tan^2(\pi/4 + \phi/2)]$  is the threshold effective stress above which rock failure (i.e., breakout) will occur (Zoback et al. 1985). For the given rock strength properties ( $C_0 = 20.7$  MPa and  $\phi = 25^\circ$ ) and using the same overburden, pore pressure and wellbore pressure as shown in Fig. 10a, the sinusoidal curves shown in Fig. 10c are constructed by varying only the values of the two horizontal principal stresses. It is theorized that when the tangential stress exceeds  $C^*$ , borehole wall failure, i.e., the

**Fig. 10** **a** Stress polygon that is constructed with  $S_v = 35.17$  MPa,  $P_p = 20.7$  MPa and the coefficient of friction of an optimally oriented fault plane ( $\mu = 0.6$ ). The shear failure lines that define the range (hatched polygon ABCD) of possible magnitudes of  $S_h$  and  $S_H$  are for the case of breakouts (breakout width,  $\theta_b = 50^\circ$ ) observed at a specific depth of a vertical borehole having a wellbore pressure ( $P_m$ ) = 24.8 MPa, and with an intact rock having Biot's coefficient ( $\alpha$ ) = 1.0, uniaxial compressive strength ( $C_o$ ) =  $20.7 \pm 3$  MPa and internal friction angle ( $\phi$ ) =  $25^\circ$ . Increasing  $P_m$  to 29 MPa but keeping other parameters results in the shift of the failure lines upward indicated by the dotted polygon EFGH. **b** The tensile failure lines that define the range (hatched polygon A'B'C'D') of possible magnitudes of  $S_h$  and  $S_H$  are for the case of drilling-induced tensile fractures (DITFs) drawn with tensile strengths of 0 and 10 MPa together with the stress and pressure inputs used in (a). Increasing  $P_m$  to 29 MPa but keeping other parameters shifts the failure lines downward indicated by the dotted polygon E'F'G'H'. **c** Variations of tangential stresses at the borehole wall as a function of circumferential angle ( $\theta$ ) by varying  $S_h$  and  $S_H$  but using the same  $S_v$ ,  $P_p$  and  $P_m$  as 10a. Compressive failure (i.e., breakouts) will occur over the  $\theta_b$  at the borehole wall where the tangential stress ( $\sigma_{\theta\theta}$ ) is greater than the rock strength,  $C^* [= C_o + \sigma_3 \tan^2(\pi/4 + \phi/2)]$ . The rock strength parameters used are  $C_o = 20.7$  MPa and  $\phi = 25^\circ$ . All the stress states ( $S_H$  and  $S_h$ ) used yield the same breakout width of  $\theta_b = 50^\circ$ , suggesting non-uniqueness in estimating  $S_H$  and  $S_h$

development of breakouts will occur. From Fig. 10c, we note that all the stress states used in the simulation produce the same breakout width of  $\theta_b = 50^\circ$ , suggesting there can be many combinations of minimum and maximum horizontal stresses to generate the same failure characteristics for the vertical well. In other words, any combination of minimum and maximum horizontal stresses within the polygon ABCD is a possible stress state that satisfies the given failure condition. This non-uniqueness of the solution renders the estimation of horizontal principal stresses difficult in a vertical well without additional information on  $S_h$ .

To overcome the need of knowing the  $S_h$  magnitude from field measurements in advance when constraining the  $S_H$  using the standard stress polygon method, Song et al. (2016) and Song and Chang (2017) developed a statistical methodology from which the minimum and maximum horizontal principal stresses ( $S_h$  and  $S_H$ ) are simultaneously estimated in vertical wellbores. In this paper and for brevity, we only briefly discuss the methodology. For details on the methodology, the papers by Song et al. (2016) and Song and Chang (2017) should be referred. A few assumptions are made in the statistical method including vertical principal stress, homogeneous, isotropic and linear elastic rock formations, and the Earth crust is in equilibrium conditions; in situ stresses do not exceed the frictional strength of preexisting weakness planes (e.g., fault).

In the statistical analysis, the entire depth of the borehole along which breakouts have developed is first subdivided into several intervals. For each of the depth intervals, a statistical analysis is performed to estimate the magnitudes of both horizontal principal stresses. Figure 11 shows a



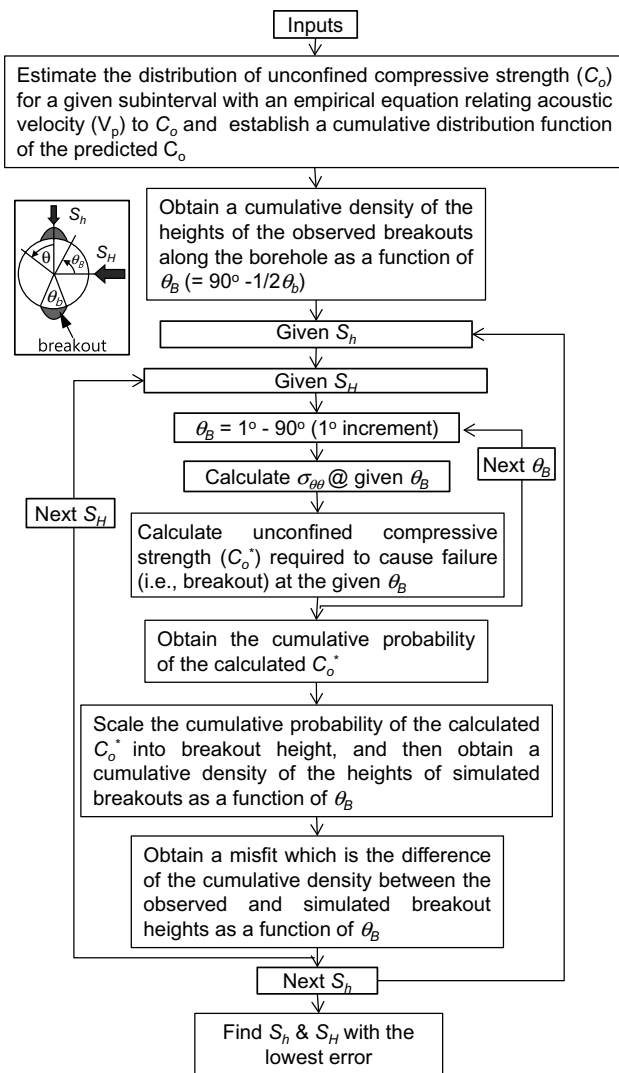


**Fig. 11** Flowchart illustrating the statistical method of constraining the two horizontal principal stresses simultaneously

flowchart describing the methodology. In short, it is a grid-searching technique in which a series of wellbore failure analyses are performed with a given set of  $S_h$  and  $S_H$ , and the solution is obtained when the lowest misfit between the observed and simulated breakout height as a function of breakout width is attained. The method requires the input of many geomechanical parameters including vertical principal stress ( $S_v$ ), pore pressure ( $P_p$ ), wellbore pressure ( $P_m$ ), acoustic log (for continuous profiling of rock strength parameters along the borehole), rock strength parameters from laboratory measurements (uniaxial compressive strength,  $C_o$ , and internal friction angle,  $\phi$ ; for calibrating log-based rock strength parameters), breakout width ( $\theta_b$ ) and breakout height (depth-related elongation of breakout width along the wellbore) observed from an image log.

The vertical stress ( $S_v$ ), pore pressure ( $P_p$ ) and wellbore pressure ( $P_m$ ) used in the analysis are referenced at the middle of each depth section. In addition, a profile of uniaxial compressive strength along each depth interval is required. The uniaxial compressive strength is estimated using an empirical equation that relates  $C_o$  to acoustic velocity, and is calibrated against laboratory core measurements (Chang et al. 2006). Figure 12a shows a histogram of predicted uniaxial compressive strengths for the depth interval 350–380 m, which is one of the nine 30-m subsections (see Sect. 4.2). The rock strengths range from 8 to 18 MPa with an average of  $\sim 11$  MPa. The variation of the predicted rock strength has been approximated by a lognormal probability density function to account for its skewness, and by integrating the lognormal probability distribution function, a cumulative density function of  $C_o$  is obtained (Fig. 12a).

Figure 12b shows the distribution of breakout heights (depth-related elongation of breakout width along the borehole) observed on the image log along the depth interval of 350–380 m, as a function of breakout angle ( $\theta_B = 90^\circ - \text{half of the breakout width}$ ). A cumulative distribution of the heights of breakouts as a function of  $\theta_B$  is obtained and then compared with the height distribution of simulated breakouts (Fig. 12c).

For a given set of  $S_h$  and  $S_H$ , the tangential stress at a point located at an angle  $\theta_B$  away from the direction of maximum horizontal principal stress is calculated. Using the Coulomb failure criterion, the compressive strength ( $C_o^*$ ) required to cause shear failure (i.e., breakout) at the point is then calculated. The Coulomb failure criterion is expressed:  $\sigma_1 = C_o + \sigma_3 \tan^2(\pi/4 + \phi/2)$ . Replacing ( $\sigma_1 = \sigma_{\theta\theta}$ ,  $\sigma_3 = \sigma_{rr}$  and  $C_o = C_o^*$ ) and rearranging the criterion gives  $C_o^* = \sigma_{\theta\theta} - \sigma_{rr} \tan^2(\pi/4 + \phi/2)$  at which shear failure occurs at the circumferential location. This is followed by establishing a cumulative probability of the calculated  $C_o^*$  from the cumulative probability function obtained for the uniaxial compressive strength ( $C_o$ ) estimated using an acoustic-based empirical relation. The same calculation is repeated with a  $1^\circ$  increment in  $\theta_B$ , and the calculation cycle continues to the point where no breakout is observed or when  $\theta_B = 90^\circ$ .

When the computation cycle is completed, the cumulative probability of the calculated  $C_o^*$  is scaled the breakout height by multiplying the cumulative probability by the depth interval along which breakouts are formed to obtain a cumulative height function of simulated breakouts as a function of  $\theta_B$  as shown in Fig. 12c (see the curves). Subsequently, comparing the cumulative breakout height distribution of simulated and observed breakouts as a function of  $\theta_B$  gives an error (or misfit) that is the difference between the two functions. The calculation then moves to a next value of  $S_H$  and  $S_h$ , and this grid-searching continues until the computation loop has been completed for the preset values of  $S_h$  and  $S_H$ .

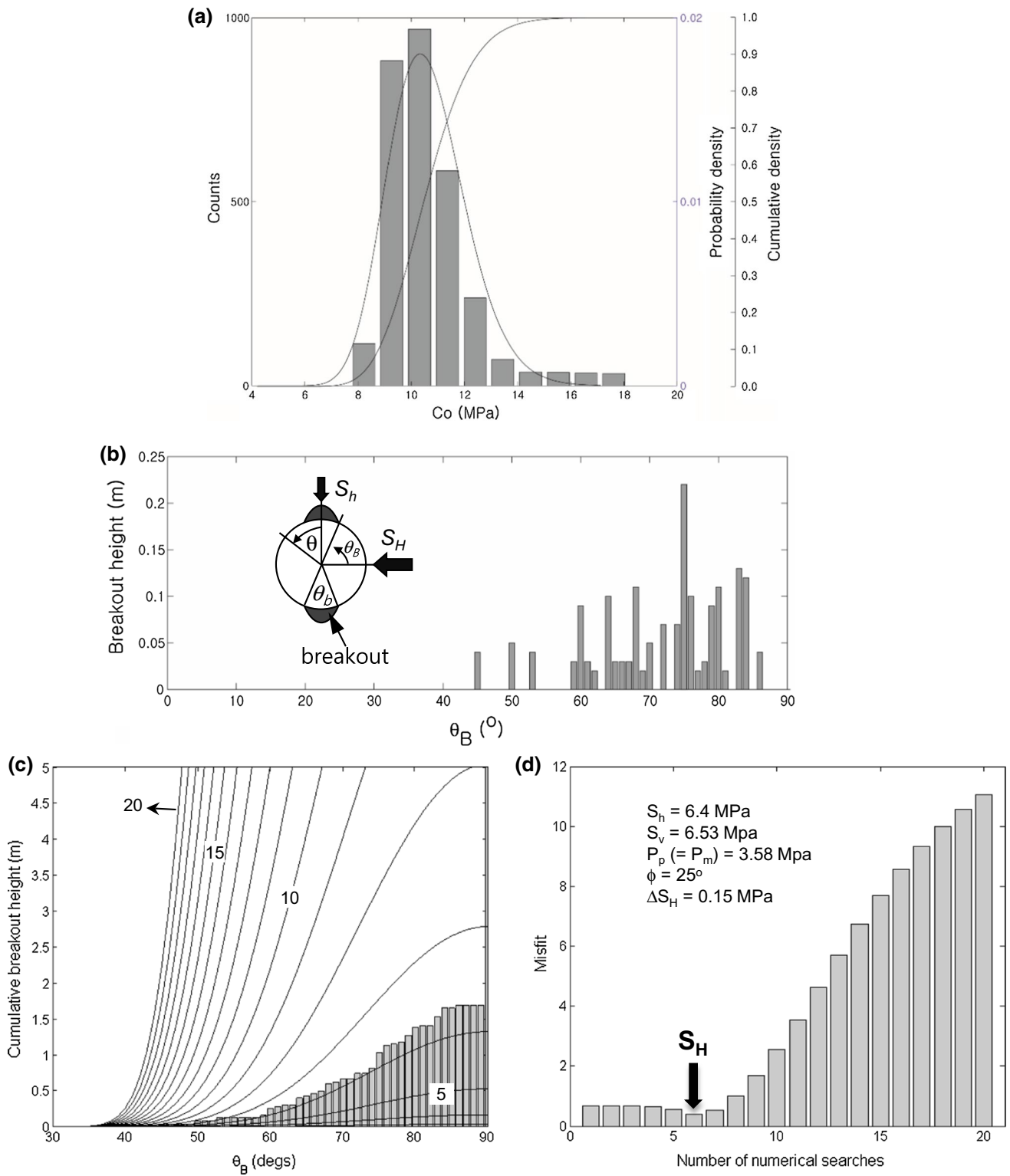


**Fig. 12** **a** Histogram of uniaxial compressive strengths ( $C_o$ ) predicted for the depth interval of 350–380 m using an acoustic velocity-based empirical relation, and the normal and cumulative probability distribution functions representing the variations of the strength parameter. **b** Borehole breakout heights as a function of  $\theta_B$  ( $= 90^\circ - 1/2 \theta_b$ , measured from the  $S_H$  direction) observed along the

depth interval of 350–380 m. **c** Cumulative height of observed breakouts (histogram) and simulated breakouts (curves) as a function of  $\theta_B$ . **d** Variation of misfits as a function of numerical searches for the case in which  $S_h$  is kept constant at 5.5 MPa, while  $S_H$  is varied at an increment of 0.2 MPa. The misfit is the difference between the cumulative height of simulated and observed breakouts shown in (c)

Figure 12d shows a result of such a calculation in which  $S_h$  is fixed at a constant value of 6.4 MPa, but  $S_H$  is varied by 0.15 MPa increments in each trial. A total of 20 searches were made. The result shows that the misfit (or error) varies with trials. By having a sufficiently large number of  $S_h$  and  $S_H$  sampling sets, a matrix of misfits can be generated, and the set of  $S_h$  and  $S_H$  giving the lowest misfit is the best-fit solution.

#### 4.2 In Situ Stress Magnitudes Estimated by the Statistical Approach

Using the proposed statistical method, we attempted to estimate the magnitudes of in situ horizontal principal stresses along the study borehole where field stress measurements were carried out with a series of hydraulic fracturing tests. The results from the statistical approach are then compared to the field measurements. For the statistical analysis, we first divided the entire depth of the borehole (from 200 m to the target depth where breakouts formed) into subintervals at 30-m-deep intervals (i.e., 200–230, 230–260, 260–290, 290–320, 320–350, 350–380, 380–410, 410–440, 440–470 m). A total of nine subsections were defined, but one subsection (410–440 m) was discarded due to the absence of breakouts along the depth interval.

The required inputs that are derived from various sources include vertical principal stress, pore pressure, breakout width, breakout height along the borehole and rock strength parameters. The vertical stress and pore pressure are obtained from the stress profiles shown in Fig. 6 and are referenced to the mid-depth of each subsection as an average value for the depth interval. The width and height of breakouts are obtained from an image log recorded by a BHTV. Figure 12b shows an example of the distribution of breakout heights against breakout widths measured along the depth interval of 350–380 m.

Although the estimation of the aforementioned input parameters is relatively straightforward, characterizing a continuous profile of rock strength parameters (i.e., uniaxial compressive strength and internal friction angle) along the borehole is probably the most challenging. This is because the rock type along the borehole changes with depths at a scale from a few tenths of a centimeter to a few meters. Even within the same lithology, the mineral composition, grain size, porosity and other rock micro-characteristics can vary, which can ultimately result in different mechanical properties. Due to the scale differences, it is common practice in the petroleum industry to predict rock strength parameters, which are required for wellbore stability analyses along a deep borehole drilled in a sedimentary basin, using empirical relations between rock strength parameters and wellbore geophysical logs (e.g., acoustic velocity) (Chang et al. 2006). The estimated rock strength parameters are then calibrated,

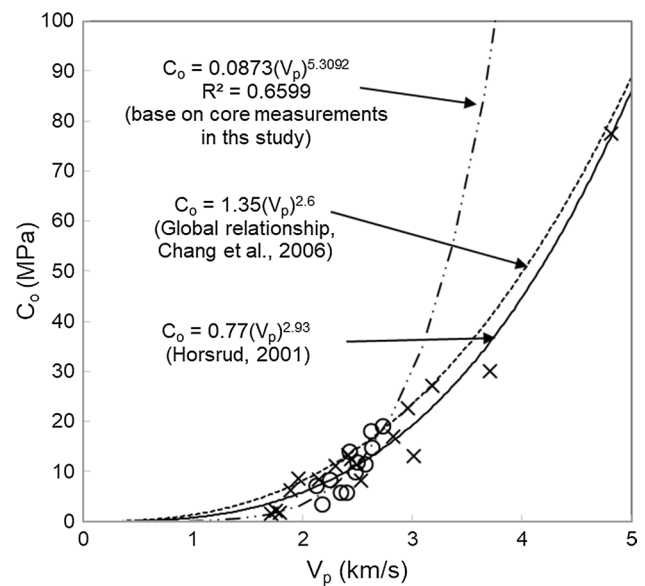
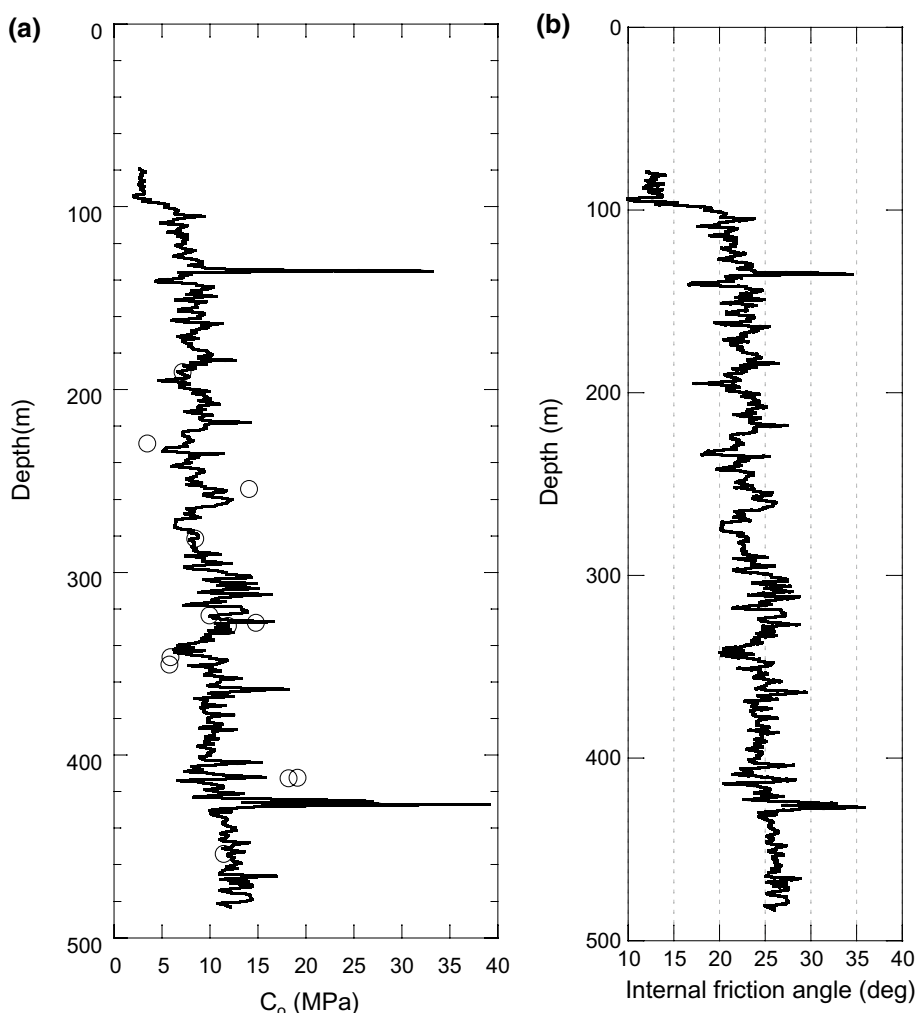


**Fig. 13** Unconfined compressive strength ( $C_o$ ) measurements vs. acoustic velocity ( $V_p$ ) and empirical relationships relating  $C_o$  to  $V_p$ . Open circles represent  $C_o$  measured on cores extracted from this study borehole and  $V_p$  measured with acoustic logging at the depth of the study borehole where the tested cores are extracted. The broken line represents the empirical equation established based on the unconfined compressive strengths measured in this study. Cross marks represent  $C_o$  and  $V_p$  measured on cores mainly from the North Sea. The solid line represents the empirical relationship proposed by Horsrud (2001) based on his core measurements. A global relationship (dotted line) is also shown as a reference (see Table 2 in Chang et al. 2006)

if available, against core measurements, which is important to account for the local conditions (e.g., different shale types, geographic locations).

An acoustic velocity log is available in the study borehole for such a prediction (Fig. 4). In addition, cores from the surface to the target depth were available for material tests. Laboratory core measurements (i.e., unconfined compression test) were conducted on fully saturated shale samples that were cut and sealed soon after extracting cores from the borehole to maintain their in situ saturation, and then immediately transported to the laboratory. Figure 13 shows core measurements and their relevant empirical relations. Open circles represent the core measurements done in this study, and cross marks are from Horsrud (2001). As seen, the core measurements of this study fit well to those from Horsrud (2001) and can be reasonably predicted with the Horsrud's empirical relation (solid line). This agreement is impressive in spite of the difference in geographic location, suggesting that Horsrud's relationship can be applied to estimate the rock strength in this study. A relationship similar to Horsrud's is the global relation (dotted line), which appears perhaps to also be usable, but would slightly overestimate the rock strength as shown.

**Fig. 14 a** Profiles of uniaxial compressive strength ( $C_o$ , line) established from the Horsrud (2001) empirical relation and core measurements (open circles), showing a relatively good agreement between the two independent derivations. The predicted  $C_o$  approximately increases linearly with depth and vertically varies within a range of 6–13 MPa, indicating lithology changes. **b** Profile of internal friction angle ( $\phi$ ) estimated using the acoustic-based empirical relation proposed by Lal (1999), and the variation is between 20° and 30°



On the other hand, the empirical relationship (broken line) established based only on the core measurements of this study appears to be very different from the other relations. It is because the  $V_p$  range of the tested cores (2.1–2.7 km/s) is relatively narrow in this study compared to that of Horsrud (2001). This suggests that the relation would work well within the  $V_p$  range of the tested cores, but not outside of it. In particular, the rock strength would be extremely overestimated in the  $V_p$  range greater than  $\sim 2.7$  km/s. This would limit the application of the empirical equation over the entire depth of the study borehole along which the  $V_p$  varies between 1.5 and 3.5 km/s (Fig. 4b).

Horsrud’s empirical relation was originally established with core measurements on mostly high porosity tertiary shales mainly from the North Sea. Being conscious of the large natural variation of shale properties and constituents, one must exert some care when using a relation developed for a different geographic location. A validation of such an application in a different geological setting can be obtained through testing of the relation. It is necessary to fully test the relation against core measurements, but we just have made

the comparison here as our best due to the given data measured over the relatively narrow range of  $V_p$ . Due to the limitation and the best performance of Horsrud’s relation among the multiple choices available for determining rock strength parameters from well logs (Chang et al. 2006), we selected the Horsrud’s (2001) relation to obtain the range of uniaxial compressive strengths along the borehole (Fig. 14a). The estimated unconfined compressive strength increases approximately linearly with depth, indicating a normal compaction of the sedimentary rocks. The strength varies within the range of  $\sim 5$  to  $\sim 17$  MPa, and the depth-related or vertical variations suggest that the properties of rock formation are changing with depth (Fig. 14a). Uniaxial compressive strengths from core measurement are replotted in Fig. 14a as open circles, and comparison between the core-based and log-based uniaxial compressive strengths shows that  $C_o$  prediction using the empirical relation agreed reasonably well with the physical measurements.

In addition to uniaxial compressive strength, an internal friction angle ( $\phi$ ) is also required as another strength parameter for the statistical approach. We used the empirical

relation proposed for shaly formations by Lal (1999) to estimate the variation of the internal friction angle with depth as shown in Fig. 14b. The internal friction angle of the rock varies mostly between 20° and 30°, and this range is typical for unconsolidated or poorly consolidated weak shales (Chang et al. 2006). Similar to uniaxial compressive strength, the log-based internal friction angle estimation must also be calibrated against laboratory measurements. However, the calibration was not carried out because triaxial test data were not available.

Nonetheless, from the Coulomb failure criterion [ $\sigma_1 = C_o + \sigma_3 \tan^2(\pi/4 + \phi/2)$ ], we note that the influence of the internal friction angle on the additional strength may not be significant in a case in which the borehole pressure ( $P_m$ ) is close to hydrostatic. As stated, the study borehole was drilled with water so that the  $P_m$  is close to hydrostatic and is almost balanced with the formation pressure ( $P_p$ ) which is also hydrostatic (Fig. 6), i.e.,  $P_m \approx P_p$ . In such a case, the effective borehole radial stress acting at the borehole wall, which is a principal stress, is considerably lower or perhaps close to zero (i.e.,  $\sigma_{rr} = \sigma_3 = P_m - \alpha P_p \approx 0$ , where  $\alpha$  is Biot's coefficient and is often assumed to be 1.0 for unconsolidated formations). Thus, the effect of uncertainty in the internal friction angle caused by no calibration is much less significant than the uncertainty of  $C_o$ . In other words, when the effective radial stress is close to zero ( $\sigma_{rr} = \sigma_3 \approx 0$ ), a small uncertainty in the  $\phi$  compared to that of  $C_o$  that is relatively much larger does not significantly affect the overall rock strength as indicated by the Coulomb criterion. Based on this argument, we chose a constant internal friction angle of 25° for the entire depth interval in the analysis.

Using the statistical methodology and for the given input parameters described above, we estimated  $S_h$  and  $S_H$  for each subsection. An example of the result from the statistical analysis (i.e., grid-searching algorithm) conducted for subsection 350–380 m is shown in Fig. 15. Figure 15a shows a contour of misfits generated from numerical trials for all the preset values of  $S_h$  and  $S_H$  within the stress polygon defined by  $\mu = 0.6$ ,  $S_v = 6.53$  MPa and  $P_p = 3.58$  MPa. The misfit is the difference between the observed and simulated cumulative breakout heights as a function of  $\theta_b$  ( $= 90^\circ - \text{half of breakout width}$ ). Numerical trials, for example, carried out along line A–A' of Fig. 15a are shown in Fig. 12c and d.  $S_h$  is fixed at  $\sim 6.4$  MPa (along the line), but  $S_H$  is changed for each simulation. The simulated cumulative breakout height (i.e., curves in Fig. 12c) at the sixth trial of a total of 20 simulations is the best matched and agrees well with the observed one (i.e., histogram) (Fig. 12c). This is also illustrated in Fig. 12d as the misfit at the sixth trial is the lowest among the 20 simulations. The simulation is repeated with different fixed values of  $S_h$  but varying  $S_H$  at each fixed  $S_h$  value over the entire stress polygon. Misfits for all sets of

$S_h$  and  $S_H$  within the polygon are obtained, and a set of  $S_h$  and  $S_H$  with the lowest misfit is identified. The cooler color (blue) represents a relatively small misfit. The white dot in Fig. 15a represents the optimum set of  $S_h$  and  $S_H$  values that yield the lowest misfit (equivalent to that of the sixth trial in Fig. 12c and d), meaning at the optimum set of horizontal principal stresses, the cumulative density function of simulated breakout heights as a function of  $\theta_b$  is in best agreement with the observed ones (Fig. 15b). Figure 15c shows an expanded or close-up view of the box indicated in Fig. 15b.

A compilation of the results of statistical analyses that yield the best sets of  $S_h$  and  $S_H$  for the individual subsections is shown in Fig. 16. As with the case of the hydraulic fracturing tests, the stress state at the study site derived from the statistical approach is a strike-slip faulting regime. The average gradients of horizontal principal stresses estimated by the statistical approach generally agreed well with those estimated by the hydraulic fracturing stress measurements. The average gradient of  $S_h$  from the statistical approach is 15.91 MPa/km, which is in good agreement, albeit slightly higher than the  $S_h$  gradient of 15.67 MPa/km measured by field hydraulic fracturing tests. On the other hand, the average gradient of  $S_H$  estimated from the statistical approach is 19.74 MPa/km, which is slightly higher than the hydraulic fracturing estimation of 20.43 MPa/km.

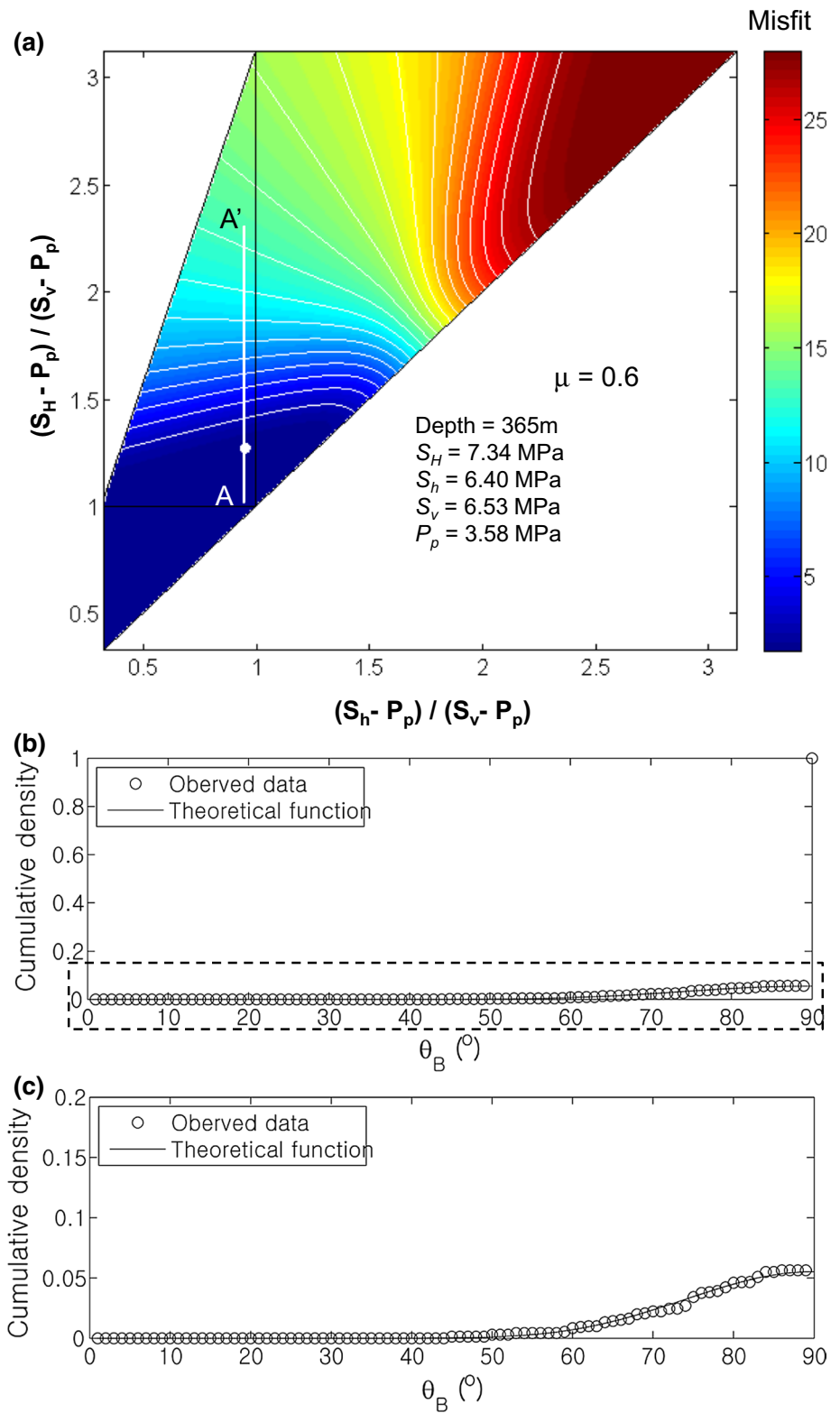
The discrepancy in the  $S_H$  gradient between the two methods is attributed to the one “outlier” that overestimate the  $S_H$  magnitudes at the subsection 200–230 m. In the statistical analysis, the magnitudes of horizontal principal stresses are strongly dependent on rock strength parameters, particularly the uniaxial compressive strength. The high  $S_H$  magnitudes in the subsections of interest appear to be related to the overestimation in the uniaxial compressive strength. These higher-than-expected  $S_H$  values also indicate that a correct estimation of the rock strength is critical for the accuracy of stress quantification using the statistical approach. Nevertheless, the horizontal principal stress estimations using the statistical methodology correspond fairly well to the field measurements, suggesting that the statistical approach can be a viable method for in situ stress characterization in vertical wells.

## 5 Discussion

We attempted a statistical approach to concurrently estimate the magnitude of both horizontal principal stresses ( $S_h$  and  $S_H$ ). In the statistical method, to consider the full range of possible stress states in the field, we constructed a stress polygon using Eq. 1 that represents the possible range of  $S_h$  and  $S_H$  defined by a coefficient of sliding friction,  $\mu = 0.6$ , vertical stress ( $S_v$ ) and pore pressure ( $P_p$ ). A regularly spacing grid parallel to the  $S_h$  and  $S_H$  axes was put on the stress



**Fig. 15** **a** Estimations of horizontal principal stresses using the statistical analysis for the depth interval of 350–380 m. **b** Cumulative density function of observed and simulated break-out heights for the horizontal principal stresses that have the lowest misfit indicated by the white dot on **(a)**. **c** Close-up view of the boxed area on **(b)**



polygon, and then, the stress states at the intersecting grid points within the polygon were sampled. All the sampled stress states were then used in the statistical method.

Compared to the stress polygon technique, the statistical method has the advantage that principally it does not require the knowledge of the  $S_h$  magnitude in advance. From Fig. 10a, we noted the possible range of horizontal stresses

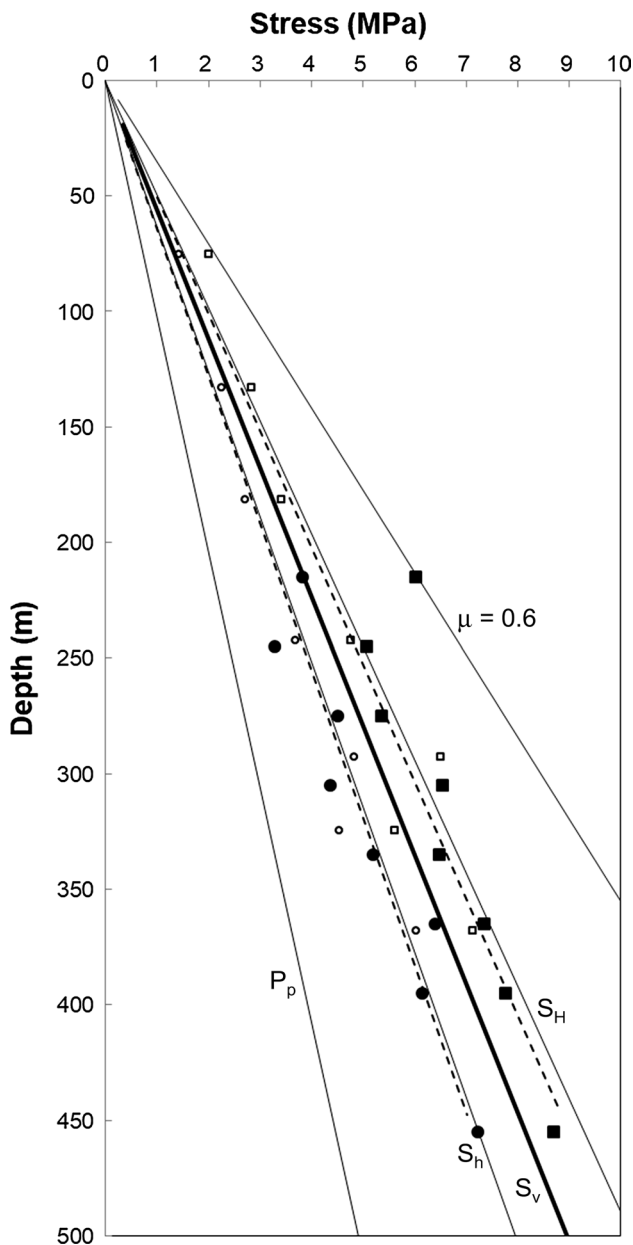


**Fig. 16** Profiles of in situ horizontal stresses measured and derived from field hydraulic fracturing tests (open circles— $S_h$ , open rectangles— $S_H$ ) and estimated by the statistical method (closed circles— $S_h$ , closed rectangles— $S_H$ ). The broken and solid lines represent the trend lines of horizontal principal stresses from field measurements (broken lines) and estimations by the statistical method (solid lines), respectively

is represented within the polygon ABCD for the given input parameters from a vertical well. Within the polygon, there are theoretically a wide range of combinations of horizontal principal stresses that can yield the same failure features (e.g., breakout width) for the prescribed range of input rock strengths. In addition, the possible spread of minimum horizontal stress is fairly wide, ranging from 0.32 to 1.0

of  $S_v$  compared to the  $S_v$ -normalized maximum horizontal stresses. For this reason, the minimum horizontal principal stress in general must be known in advance to reduce the uncertainty when using the stress polygon technique to constrain the maximum horizontal principal stress.

In contrast, as shown in Fig. 15a, the statistical method uses the combinations of possible horizontal stresses within the stress polygon by means of the grid-searching technique to identify a combination that has the lowest misfit in width and height between the observed and simulated breakouts (Fig. 15a). Essentially, the approach estimates the minimum and maximum horizontal principal stresses simultaneously; in that sense, the information on minimum horizontal stress is theoretically not required in advance. However, the knowledge of the minimum horizontal stress serves as a means to validate the accuracy of the principal stresses estimated from the statistical method.

Fundamentally, a good-quality data set is essential in the statistical method. It is known that the widths of breakouts in competent rocks do not change with time, whereas the width of breakouts in weak muddy sedimentary rocks can widen with time (Moore et al. 2011). Care should be exercised in cases where the width of breakouts formed in such formations is used for characterizing in situ stresses. The use of a breakout width wider than that caused by a stress-induced failure will result in an overestimation of the maximum horizontal stress. In such formations, it is critical to run an image log immediately after drilling or while drilling, and the latter is best served with a logging-while-drilling (LWD) image logs. Another input parameter that can significantly affect the result is rock strength, particularly the unconfined compressive strength. For this reason, it is highly recommended to calibrate the log-based rock strength parameter predictions against core measurements. Additionally, in the case where the lithology along the wellbore varies significantly with depth, such as when drilling through interbedded sand–shale and/or carbonate–shale sequences, it is recommended to use several empirical relations, one for each lithology for rock strength estimations.

As shown in Fig. 16, the in situ stresses estimated with the statistical approach are in fairly good agreement with the stresses determined by the field hydraulic fracturing tests. This suggests that based on only a limited data set, the statistical approach could be viable for estimating the horizontal principal stress magnitudes. However, for the method to be used as a regular engineering tool, the reliability of the statistical methodology needs to be further validated by more field data. For this purpose, it is necessary to have known in situ stress states from other means, well-developed breakouts along a vertical borehole and laboratory core measurements, all of which may not exist in a single well. To resolve this lack of a complete data set from a single well, it is common practice to use data from neighboring

boreholes in the same field, assuming that the far-field stress direction and the principal stress ratios are constant throughout the field. When more data become available from other fields, the accuracy of the statistical method would be further improved.

Peska and Zoback (1995) proposed an approach that can be used to simultaneously constrain the magnitude of both horizontal stresses in deviated wellbores using additional information on the circumferential location of failures around the wellbore. The method does not require a prior knowledge of the  $S_h$  magnitude as well. However, there is a fundamental difference between the statistical method used in this study and Peska's and Zoback's method. In the statistical method, the breakout geometry (i.e., breakout width) is related to the relative magnitude of horizontal stresses, while in Peska's and Zoback's method, the circumferential location of breakouts and/or DITFs is related to not only the horizontal principal stresses but also the vertical component. Schoenball et al. (2016) recently employed Peska's and Zoback's methodology to constrain the magnitude of horizontal stresses in a geothermal field where near-vertical and deviated wells were drilled and wellbore failures were observed in both wellbore types. They showed that the methodology worked well in the deviated wellbores but failed in the vertical wells because the methodology cannot distinguish the different stress regimes only from the circumferential location of wellbore failures in vertical wells. So the statistical method is, so far, the only method to be used to estimate concurrently both horizontal principal stresses in the case that both of them are not known in a vertical borehole.

In this study, the statistical method has been successfully applied to a vertical borehole to estimate both in situ horizontal principal stresses. The results suggest that the statistical method can be a viable method for constraining the horizontal stresses in vertical wellbores, particularly for the case where no prior information on the  $S_h$  magnitude and stress regime is available. It is anticipated that the statistical method can also be applied to non-vertical holes in the most general case with multiple stress transformations between different coordination systems as had done by Mastin (1988) and Peska and Zoback (1995). Although the statistical method is theoretically applicable to non-vertical holes, its applicability to such boreholes with another degree of freedom (breakout location) needs to be further evaluated with data available from inclined wellbores.

## 6 Conclusions

A set of hydraulic fracturing tests were carried out at selected depths along a vertical borehole. The pressure data

recorded during the tests were analyzed to identify the  $S_h$  magnitude. Assuming a non-fluid penetrating condition and using key pressure parameters identified during the tests, the  $S_H$  magnitude was estimated using the Kirsch's solution. The field stress measurements indicate that the state of in situ stresses at the site corresponds to the strike-slip faulting regime.

In parallel with the hydraulic fracturing-based horizontal principal stress characterizations, we also estimated the in situ stresses at the same site by employing a statistical method (recently proposed by Song et al. 2016 and Song and Chang 2017) that can simultaneously estimate the magnitude of in situ horizontal stresses with other known relevant data. We then compared the principal stress estimations from the statistical method to those determined by the hydraulic fracture stress measurements to evaluate the validity of the statistical method.

The statistical methodology is a grid-searching algorithm that uses a number of combinations of least and maximum horizontal principal stresses within a stress polygon defined by Anderson faulting and Coulomb failure theories. For each individual set of  $S_h$  and  $S_H$ , the algorithm finds the misfit that is the difference between simulated and observed breakout heights as a function of breakout angle ( $\theta_B$ ). The set of  $S_h$  and  $S_H$  that produces the lowest misfit is correspondingly the best solution to the problem.

Many input parameters are required for the application of the methodology. The width and height of borehole breakouts were obtained from an acoustic image log recorded along the study borehole. Rock strength parameters, another critical input, were estimated using acoustic-based empirical relations, which were later calibrated with core measurements.

Given the uncertainty inherent in some of the input parameters, the results of the statistical method agreed well with the field stress measurements. An important advantage of the statistical method is that, unlike the standard stress polygon technique that requires the knowledge of  $S_h$  for vertical wells, the proposed statistical approach derives the two horizontal principal stresses simultaneously. Although  $S_h$  is not required in the statistical method, the knowledge of  $S_h$  in advance even at only a single depth is particularly useful to verify the robustness of the statistical estimation.

**Acknowledgements** This research was partially supported by the Basic Research Project of the Korea Institute of Geoscience and Mineral Resources (KIGAM) and by the project titled "International Ocean Discovery Program (K-IODP)" funded by the Ministry of Oceans Fisheries, Korea. We appreciate the comments and suggestions provided by the anonymous reviewers and the Co-Editor of the journal.

## References

- Anderson EM (1951) The dynamics of faulting and dike formation with application to Britain. Edinburgh, Oliver and Boyd
- Baumgartner J, Zoback MD (1989) Interpretation of hydraulic fracturing pressure–time records using interactive analysis methods. *Int J Rock Mech Min Sci Geomech Abstr* 26(6):461–469
- Bell JS, Gough DI (1979) Northeast-southwest compressive stress in Alberta: evidence from oil wells. *Earth and Planet Sci Lett* 45:475–482
- Bredehoeft JD, Wolff RG, Keys WS, Shuter E (1976) Hydraulic fracturing to determine the regional in situ stress field, Piecance Basin, Colorado. *Geol Soc Am Bull* 87:250–258
- Brudy M, Zoback MD (1999) Drilling-induced tensile wall-fractures: implications for determination of in situ stress orientation and magnitude. *Int J Rock Mech Min Sci* 36:191–215
- Brudy M, Zoback MD, Fuchs K, Rummel F, Baumgartner J (1997) Estimation of the complete stress tensor to 8 km depth in the KTB scientific drill holes: implications for crustal strength. *J Geophys Res* 102(B8):18453–18475
- Byerlee JD (1978) Friction of rock. *Pure appl Geophys* 116:615–626
- Chang C, Zoback MD, Khaksar A (2006) Empirical relations between rock strength and physical properties in sedimentary rocks. *J Petrol Sci Eng* 21:223–237
- Chang C, McNeill LC, Moore JC, Lin W, Conin M, Yamada Y (2010) In situ stress state in the Nankaiaccretionary wedge estimated from borehole wall failures. *Geochem Geophys Geosyst* 11:Q0AD04. [10.1029/2010GC003261](https://doi.org/10.1029/2010GC003261)
- Chang C, Jo Y, Oh Y, Lee T, Kim K (2013) Hydraulic fracturing in situ stress estimations in a potential geothermal site, Seokmo Island, South Korea. *Rock Mech Rock Eng.* [10.1007/s00603-013-0491-7](https://doi.org/10.1007/s00603-013-0491-7)
- Chough SK, Hwang IG, Choe MY (1990) The Miocene Doumsan fan-delta, South Korea: a composite fan-delta system in back-arc margin. *J Sediment Petrol* 67:130–141
- Doe TW, Hustrulid WA, Leijon B, Ingvald K, Strindell L (1983) Determination of the state of stress at the Stripa mine, Sweden. Hydraulic fracturing stress measurements. National Academy Press, Washington, pp 119–129
- Enever JR, Chopra PN (1986) Experience with hydraulic fracture stress measurements in granite. In: Proceedings of international symposium on rock stress and rock stress measurement, CENTEK Publications, Lulea, pp 411–420
- Fairhurst C (2003) Stress estimation in rock: a brief history and review. *Int J Rock Mech Min Sci* 40:957–973
- Gronseth JM, Kry PR (1983) Instantaneous shut-in pressure and its relationship to the minimum in situ stress. Hydraulic fracturing stress measurements. National Academy Press, Washington DC, pp 230–257
- Guo F, Morgenstern NR, Scott JD (1993) Interpretation of hydraulic fracturing breakdown pressure. *Int J Rock Mech Min Sci Geomech Abstr* 30(6):617–626
- Haimson BC (1978) The hydrofracturing stress measuring method and recent field results. *Int J Rock Mech Min Sci Geomech Abstr* 15:167–178
- Haimson BC, Cornet FH (2003) ISRM suggested methods for rock stress estimation—part 3: hydraulic fracturing (HF) and/or hydraulic testing of pre-existing fractures (HTPF). *Int J Rock Mech Min Sci* 40:1011–1020
- Haimson BC, Fairhurst C (1967) Initiation and extension of hydraulic fracture in rocks. SPE1701 In: SPE Third Conference on Rock Mechanics held in Austin, Texas, January 25–26, 1967
- Haimson BC, Herrick C (1986) Borehole breakouts—a new tool for estimating in situ stress? In: Paper presented at the international symposium on rock stress and rock stress measurement, Lulei University of Technology, Stockholm, Sweden
- Haimson BC, Zhao Z (1991) Effect of borehole size and pressurization rate on hydraulic fracturing breakdown pressure. In: Roegiers JC (ed) Rock mechanics as a multidisciplinary science. Balkema, Rotterdam, pp 191–199
- Hickman S, Zoback MD (2004) Stress orientation and magnitudes in the SAFOD pilot hole. *Gephys Res Lett* 31:L15S12. [10.1029/2004GL020043](https://doi.org/10.1029/2004GL020043)
- Horsrud P (2001) Estimating mechanical properties of shale from empirical correlations. *SPE Drill Completion* 16:68–73
- Hubbert SH, Willis DG (1957) Mechanics of hydraulic fracturing. *J Pet Technol* 9:153–168
- Jensen SS (2016) Experimental study of direct tensile strength in sedimentary rocks. MS Thesis, Norwegian University of Science and Technology, p 95
- Lal M (1999) Shale stability: drilling fluid interaction and shale strength. In: SPE Latin American and Caribbean Petroleum Engineering Conference held in Caracas Venezuela
- Lee MY (1991) Advances in instrumentation, data analysis, and stress calculations in hydraulic fracturing; implementation in an inclined test hole. Ph.D. Thesis, University of Wisconsin-Madison, pp 195
- Lee MY, Haimson BC (1989) Statistical evaluation of hydraulic fracturing stress measurement parameters. *Int J Rock Mech Min Sci Geomech Abstr* 26:447–456
- Ljunggren C, Chang Y, Janson T, Christiansson R (2003) An overview of rock stress measurement methods. *Int J Rock Mech Min Sci* 40:957–989
- Mastin L (1988) Effect of borehole deviation on breakout orientation. *J Geophys Res* 93(B8):9187–9195
- Moore JC, Chang C, McNeil L, Thu MK, Yamada Y, Huftile G (2011) Growth of borehole breakouts with time after drilling: implications for state of stress, NanTroSEIZE transect, SW Japan. *Geochem Geophys Geosyst* 12(4):Q04D09. [10.1029/2010GC003417](https://doi.org/10.1029/2010GC003417)
- Moos D, Zoback MD (1990) Utilization of observations of well bore failure to constrain the orientation and magnitude of crustal stresses: application to continental, deep sea drilling project, and ocean drilling program boreholes. *J Geophys Res* 95(B6):9305–9325
- Peska P, Zoback M (1995) Compressive and tensile failure of inclined wellbores and determination of in situ stress and rock strength. *J Geophys Res* 100(B7):12791–12811
- Raaen AM, Brudy M (2001) Pump-in/flowback tests reduce the estimate of horizontal in situ stress significantly. In: SPE 71367 presented at the 2001 SPE annual technical conference and exhibition held in New Orleans, Louisiana, 30 September–3 October 2001
- Raaen AM, Skomedal E, Kjørholt H, Markestad P, Okland D (2001) Stress determination from hydraulic fracturing tests: the system stiffness approach. *Int J Rock Mech Min Sci Geomech Abstr* 38:529–541
- Schmitt DR, Zoback MD (1992) Diminished pore pressure in low porosity crystalline rock under tensional failure: apparent strengthening in dilatancy. *J Geophys Res* 97:273–288
- Schoenball M, Glen JMG, Davazes NC (2016) Analysis of interpretation of stress indicators in deviated wells of the Coso geothermal field. In: SGP-TR-209, 41st workshop on geothermal reservoir engineering, Stanford University, Stanford, California, February 22–24, 2016
- Shamir G, Zoback MD (1992) Stress orientation profile to 3.5 km depth near the San Andreas Fault at Cajon Pass, California. *J Geophys Res* 97(B4):5059–5080
- Sohn YK, Son M (2004) Synrift stratigraphic geometry in a transfer zone coarse-grained delta complex, Miocene Pohang Basin, SE Korea. *Sedimentology* 51:1387–1408
- Sohn YK, Rehee CW, Shon H (2001) Revised stratigraphy and reinterpretation of the Miocene Pohang basinfill, SE Korea: sequence

- development in response to tectonism and eustasy in a back-arc basin margin. *Sediment Geol* 143:265–285
- Song I, Chang C (2017) In situ horizontal stress conditions at IODP site C0002 reflecting the tectonic evolution of the sedimentary system near the seaward edge of the Kumano basin offshore from SW Japan. *J Geophys Res Solid Earth* 122:4033–4052
- Song CW, Son M, Sohn YK, Han R, Shinn YJ, Kim JC (2015) A study on potential geologic facility sites for carbon dioxide storage in the Miocene Pohang basin, SE Korea. *J Geol Soc Korea* 51(1):53–66
- Song I, Chang C, Lee H (2016) A stochastic approach to the determination of in situ stress magnitudes from sonic velocity and breakout logging data. In: *Proceedings on the 7th international symposium on in situ rock stress, RS 2016, Tampere, Finland, May 10–12, 2016*
- Wiprut D, Zoback M, Hanssen T-H, Peska P (1997) Constraining the full stress tensor from observations of drilling-induced tensile fractures and leak-off tests: application to borehole stability and sand production on the Norwegian margin. *Int J Rock Mech Min Sci* 34(3–4):365
- Yamashita F, Mizoguchi K, Fukuyama E, Omura K (2010) Reexamination of the present stress state of the Atera fault system, central Japan, based on the calibrated crustal stress data of hydraulic fracturing tests obtained by measuring the tensile strength of rock. *J Geophys Res* 115:B04409
- Zoback MD, Haimson BC (1982) Status of hydraulic fracturing method for in situ stress measurements. In *Issues in rock mechanics*. In: *Proceedings of 23rd US symposium on rock mechanics, Society of Mining Engineers of AIME, New York*, pp 143–156
- Zoback MD, Moose D, Mastin L, Anderson RN (1985) Well-bore breakouts and in situ stress. *J Geophys Res* 90:5523–5538
- Zoback MD, Barton CA, Brudy M, Castillo DA, Finkbeiner T, Grollmund BR, Moos DB, Peska P, Ward CD, Wiprut DJ (2003) Determination of stress orientation and magnitude in deep wells. *Int J Rock Mech Min Sci* 40:1049–1076